

Citation for the published version:

Medina, N., Borissova, J., Bayo, A., Kurtev, R., Navarro-Molina, C., Kuhn, M., ... Smith, L. C. (2018). An Automated tool to detect variable sources in the Vista Variables in the Vía Láctea Survey. The VVV Variables (V⁴) catalog of tiles d001 and d002. The Astrophysical Journal, 864, [11]. DOI: 10.3847/1538-4357/aacc65.

Document Version: Accepted Version

Link to the final published version available at the publisher:

<https://doi.org/10.3847/1538-4357/aacc65>

© 2017 The American Astronomical Society. All rights reserved.

General rights

Copyright© and Moral Rights for the publications made accessible on this site are retained by the individual authors and/or other copyright owners.

Please check the manuscript for details of any other licences that may have been applied and it is a condition of accessing publications that users recognise and abide by the legal requirements associated with these rights. You may not engage in further distribution of the material for any profitmaking activities or any commercial gain. You may freely distribute both the url (<http://uhra.herts.ac.uk/>) and the content of this paper for research or private study, educational, or not-for-profit purposes without prior permission or charge.

Take down policy

If you believe that this document breaches copyright please contact us providing details, any such items will be temporarily removed from the repository pending investigation.

Enquiries

Please contact University of Hertfordshire Research & Scholarly Communications for any enquiries at rsc@herts.ac.uk

AN AUTOMATED TOOL TO DETECT VARIABLE SOURCES IN THE VISTA VARIABLES IN THE VÍA
LÁCTEA SURVEY. THE VVV VARIABLES (V⁴) CATALOG OF TILES D001 AND D002.

N. MEDINA,^{1,2} J. BORISSOVA,^{2,1} A. BAYO,^{2,3} R. KURTEV,^{2,1} C. NAVARRO-MOLINA,^{1,2} M. KUHN,^{2,1} N. KUMAR,⁴
P. W. LUCAS,⁴ M. CATELAN,^{5,1} D. MINNITI,^{6,1,7} AND L. C. SMITH^{8,9}

¹*Millennium Institute of Astrophysics (MAS), Santiago, Chile.*

²*Instituto de Física y Astronomía, Universidad de Valparaíso, Av. Gran Bretaña 1111, Playa Ancha, Casilla 5030, Chile.*

³*Núcleo Milenio Formación Planetaria - NPF, Universidad de Valparaíso, Av. Gran Bretaña 1111, Valparaíso, Chile.*

⁴*Centre for Astrophysics, University of Hertfordshire, College Lane, Hatfield, AL10 9AB, UK.*

⁵*Instituto de Física, Facultad de Física, Pontificia Universidad Católica de Chile, Casilla 306, Santiago 22, Chile*

⁶*Departamento de Ciencias Físicas, Facultad de Ciencias Exactas, Universidad Andrés Bello, Av. Fernandez Concha 700, Las Condes, Santiago, Chile.*

⁷*Vatican Observatory, V00120 Vatican City State, Italy.*

⁸*Institute of Astronomy, University of Cambridge, Madingley Road, Cambridge, CB3 0HA, UK*

⁹*Centre for Astrophysics Research, University of Hertfordshire, College Lane, Hatfield AL10 9AB, UK.*

(Dated: June 12, 2018; Received January 12, 2018; Revised May 13, 2018; Accepted May 16, 2018)

Submitted to ApJ

ABSTRACT

Time-varying phenomena are one of the most substantial sources of astrophysical information and their study has led to many fundamental discoveries in modern astronomy. We have developed an automated tool to search and analyze variable sources in the near infrared K_s-band, using the data from the Vista Variables in the Vía Láctea (VVV) ESO Public Large Survey. This process relies on the characterization of variable sources using different variability indices, calculated from time series generated with Point Spread Function photometry of sources under analysis. In particular, we used two main indices: the total amplitude ΔK_s and the eta index, η , to identify variable sources. Once variable objects are identified, periods are determined with Generalized Lomb-Scargle periodograms, and the Information Potential Metric. Variability classes are assigned according to a compromise between comparisons with VVV Templates and the period of the variability. The automated tool is applied on VVV tiles d001 and d002 and led to discovery of 200 variable sources. We detected 70 irregular variable sources and 130 periodic ones. In addition nine open cluster candidates projected in the region are analyzed, the infrared variable candidates found around these clusters are further scrutinized by cross-matching their locations against emission star candidates from VPHAS+ survey H α color cuts.

Keywords: — infrared: stars — stars: pre-main sequence — stars: variables: general — (Galaxy:) open clusters and associations: general — (Galaxy:) open clusters and associations: individual (VVV CL005, VVV CL007, VVV CL008, VVV CL009)

1. INTRODUCTION

Time-varying phenomena are arguably one of the most powerful sources of astrophysical information. In the last decades, the development of astronomical instrumentation and automation has enabled many time-domain surveys, such as for example the wide-field optical imaging surveys: the Catalina Real-time Transient Survey (Drake et al. 2009); Pan-STARRS (Kaiser et al. 2002); and GAIA (Perryman 2005). In the near future, even more ambitious programs, such as the Large Synoptic Survey Telescope (LSST, Krabbenham & Sweeney 2010) are planned to start monitoring the optical sky. While optical surveys are getting wider and deeper, the extension and the systematic exploration of the variable sky toward the infrared, is also under development, in order to better cope with the problem of the interstellar extinction. The VISTA Variables in the Vía Láctea survey (VVV; Minniti et al. 2010; Saito et al. 2012a) is one of these infrared surveys and is comparable to the optical ones both in areal and time-domain coverage (e.g., Arnaboldi et al. 2007, 2012). It has been designed to catalog $\sim 10^9$ sources, where a great part of those are expected to be variable stars. All these sources will be used to map the structure of the optically obscured Galactic disk and bulge by using some main distance indicators such as the red-clump giants and pulsating variable stars (RR Lyrae stars, classical Cepheids, anomalous Cepheids and Miras, and semi-regular variables), as well as to provide a census of Young Stellar Objects (YSOs) across the southern Galactic plane. Some focused studies have been carried out in the southern disc region in search of variable stars using these data, for example: Contreras Peña et al. (2017a,b), cataloging high amplitude variable stars, with emphasis on YSOs; Borissova et al. (2016) searching for YSOs around young stellar clusters; Dékány et al. (2015) searching Classical Cepheids in the bulge; Elorrieta et al. (2016); Gran et al. (2016); Minniti et al. (2017) focusing on the RR Lyrae stars. However, the systematic and uniform searches of the variability phenomena in the VVV disc area are still missing. On the other hand, the VVV multi-epoch observations produced a huge amount of information, a dataset of challenging size. It is highly necessary to develop tools, processes and techniques ables to perform sophisticated analysis in an automated way in order to efficiently exploit this unique dataset. In this paper we present an automated tool designed to search, classify and analyze variable sources in the near infrared K_s -band. Our tool is fed VVV tile images to extract time series and identify different types of variable sources. The main goal is to understand the behavior of K_s -band variability in large regions of the sky, with the ultimate goal of processing the 1.8 squared degrees images of the VVV observations. The identified variables will be used to derive properties in active star forming regions, to determine distances using the periodic stars with available period-luminosity relation, as RR Lyrae and Cepheids, and to identify parameters of different variables stars. The information gathered from these sources will be collected in the "VVV Variables (V^4)" catalog.

The structure of the paper is as follows: In section 2 we present the photometry and calibration process on the VVV tiles and characteristics of the extracted time series. Then in section 3 the methodology is explained, where we focus on identifying irregular and periodic variables, mainly using different variability indices and periodograms. Next in section 4, the preliminary classification of the selected sources is presented. This classification is based on principal properties of the sources, as the shape of time series and light curves, and the period in the case of variable sources. We determined general properties of selected variables sources, as characteristic features of the light curves and locations on the color-magnitude and color-color diagrams. Also, we described the environment of variable sources in the Young stellar clusters candidates projected on VVV tiles d001 and d002. Finally, in section 5 we present the catalog of variable sources in these tiles. The individual characterization of the variable objects is beyond the scope of this paper, and they will be analyzed in an up-coming work, once the follow-up spectroscopic analysis is completed.

2. THE VVV DATA

The VVV survey is an ESO Infrared Large Public survey (Minniti et al. 2010; Saito et al. 2012b) which uses the 4-meter VISTA telescope located at Cerro Paranal Observatory, Chile. The survey was designed for mapping 562 deg^2 in the Galactic bulge and the southern disk in five near-infrared broad-band filters: Z ($\lambda_{\text{eff}} = 0.87 \mu\text{m}$), Y ($\lambda_{\text{eff}} = 1.02 \mu\text{m}$), H ($\lambda_{\text{eff}} = 1.25 \mu\text{m}$), J ($\lambda_{\text{eff}} = 1.64 \mu\text{m}$), K_s ($\lambda_{\text{eff}} = 2.14 \mu\text{m}$), with a time coverage spanning over five years between 2010 and 2015 in the K_s -band. The telescope has a near-infrared camera, VIRCAM (Dalton et al. 2006), consisting of an array of 16 detectors with 2048×2048 pixels. A set of single exposures (a paw-print) are combined into a tile, covering 1.5×1.1 degrees in the sky. To cover the VVV area, the disk field was divided into 152 tiles and the bulge into 196 tiles (see Saito et al. 2012a for more details).

To test our method we choose the first two VVV disk tiles, namely d001 and d002, due to their low crowding and interstellar reddening when compared to the rest of the VVV disk area. The preliminary reduced images were retrieved

from the VISTA Science Archive¹ (VSA) database (Cross et al. 2012), keeping the quality flags. In total, we analyzed up to 55 and 41 K_s images for the tiles d001 and d002, respectively. Figure 1 represents the log of observations of the VVV tiles.

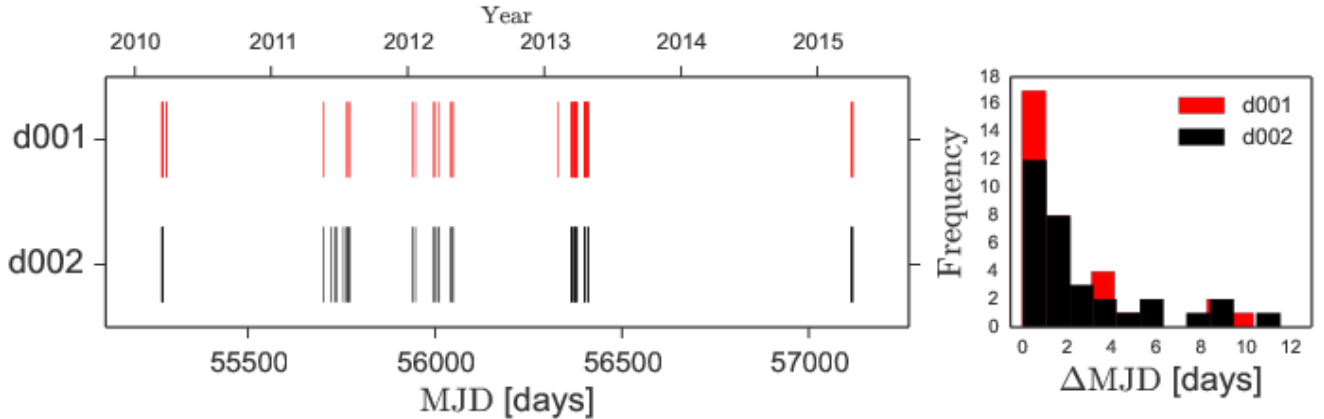


Figure 1. Left side: The log of observations of VVV tiles d001 and d002 between 2010 and 2015, based on the log representation of Rebull et al. (2014). Each photometric measurement is marked by a ‘|’ symbol. The bars are thicker in places with high cadence. Right side: Histogram of differences between consecutive observations ΔMJD . It is possible to see that the typical time interval between observations is between 0.3 and 2 days.

2.1. Photometry and calibrations

The Point Spread Function (PSF) photometry was obtained using the *Dophot* software (Schechter et al. 1993; Alonso-García et al. 2012) in all available tile images in the field of view (FoV). We based this procedure in the method explained in Navarro Molina et al. (2016). We assessed the reliability of the photometry, using the *Dophot* parameter *chi*, which quantifies the PSF quality. The sources with $chi > 3$ were rejected, due to the large associated uncertainty. The calibration process to the VISTA system was done using the aperture photometry catalogs produced by the Cambridge Astronomical Survey Unit² (CASU). We selected sources with Stellar (“-1”) or border-line stellar (“-2”) morphological classification to perform the cross-match using *STILTS* (Taylor 2006), using the catalog of the first epoch as reference with a 0.”³⁴ tolerance (VIRCAM pixel size). The conversion factors and uncertainties were estimated via a 2-sigma clipping linear fit to the *Dophot* PSF photometry vs. the CASU isolated selected sources. By following this procedure, we have found 624,983 sources in d001 and 683,643 sources in d002 in common, in K_s -band. The photometry in J and H band was performed using *Dophot* in a similar manner, i.e., using the CASU catalogs to calibrate the PSF photometry.

2.2. Cadence of the observations

As it has been pointed out, the tiles d001 and d002 accumulate up to 55 and 41 epochs observed between 2010 and 2015, respectively. Left side of Figure 1 shows the gaps, the baseline, and the maximum size of the time-step between epochs. The right side of Figure 1 shows the distribution of the difference of consecutive observations ΔMJD , zoomed up to $\Delta\text{MJD} > 12$ days. The minimum time interval between the observation is ~ 0.35 days, with distribution maximum between 0.35 and 2 days. Thus, from the time cadence of the observations, we can expect to detect variability related to timescale accretion variations, star spots, episodic accretion events, rotational modulation and variable extinction in the YSOs (Contreras Peña et al. 2017a; Rebull et al. 2014). On the other hand, VVV produces unevenly spaced light-curves, which provides its challenges, but still we expect to identify different types of periodic variability in a wide range of time-scales (see for example Elorrieta et al. 2016; Gran et al. 2016; Minniti et al. 2017).

¹ <http://horus.roe.ac.uk/vsa>

² <http://casu.ast.cam.ac.uk>

Table 1. Variability indices computed in this analysis

Set of variability indices	
Index	Reference
η index	von Neumann (1941)
Stetson J	Stetson (1996)
Stetson K	Stetson (1996)
σ_{ts}/μ ratio	Shin et al. (2009)
Classical χ^2	Rebull et al. (2014)
Total amplitude ΔK_s	Contreras Peña et al. (2017a)

2.3. The K_s -band time series

The K_s -band time series of the sources were constructed by cross-correlation of all the catalogs for all available epochs. We filtered our initial sets of time series with some ad-hoc quality and robustness criteria: 1) A minimum of 25 photometric measurements. 2) A total amplitude $\Delta K_s > 0.2$ mag, where $\Delta K_s = (K_s^{\max} - K_s^{\min})$. 3) An upper limit in flux of $K_s > 11$ mag (to avoid objects that may suffer from saturation in some VVV epoch). The first restriction represents the minimum number of epochs which allows to search for reliable periods. The second is motivated by a conservative estimation of the errors of photometry and transformation to the standard system. These initial filters reduced the source numbers obtained from photometry by approximately 30% (for example from 669825 to 433102 for d001). Moreover, the photometric measurements are prone to be affected by systematic errors that are hard to clarify and quantify, given atmospheric or instrumental problems. For example [Alonso-García et al. \(2015\)](#) reported a problem related with highly variable PSFs in the tile images, due to different geometric distortions in the combination process of the paw-print images. Thus, to remove outliers in the time series, we implement the modified Thompson τ technique, which is based on the definition shown in [Thompson \(1985\)](#). The modified Thompson τ statistic is defined as:

$$\tau = \frac{t_{\alpha/2}(n-1)}{\sqrt{n}\sqrt{n-2+t_{\alpha/2}^2}}, \quad (1)$$

where n is the number of data points, and $t_{\alpha/2}$ is the critical value of Student’s t-distribution given a confidence parameter α . For each photometric data point K_s in a time series, the standard deviation of the time series σ_{ts} and the absolute deviation $\delta_i = |K_{s_i} - \bar{K}_s|$ is calculated, where \bar{K}_s is the mean K_s magnitude. Individual photometric measurements were removed from time series when $\delta_i > \tau\sigma_{ts}$, using a confidence level of 95% (i.e. $\alpha = 0.05$). One of the consequences of this approach is that we will remove poorly sampled transients event from our time series. Figure 2 shows the performance of this method acting on a time series.

3. METHODOLOGY

In time series analysis, it is frequent to use different sets of statistics, commonly called “variability indices”, to quantify changes in luminosity with time. Depending on the definition of these indices, a population of variables that have similar behavior can be identified and one can try to separate stochastic variability from “further organized” flux variations. Examples of these indexes are the Welch-Stetson I_{ws} ([Welch & Stetson 1993](#)) and Stetson J_{Stet} and K_{Stet} indexes ([Stetson 1996](#)). This quantities have been used to identify sources that exhibit large photometric variations along the time. Defined in this manner, sources with larger J_{Stet} values are the most probable variable sources. Different authors in the literature define particular limit values of J_{Stet} for this task (such as $J_{Stet} \geq 0.55$ [Carpenter et al. 2001](#), $J_{Stet} \geq 0.9$ [Rebull et al. 2014](#)). In the literature, it is possible to find many more different indices (or features) tailored to identify different types of variable sources. Thus, deciding which index is useful to detect a specific type of variability does not only depend on the definition of the index itself, but also on the properties of the available data. Here, we briefly summarize some variability indices applicable when only one photometric band is available; and the type of variability that they can detect.

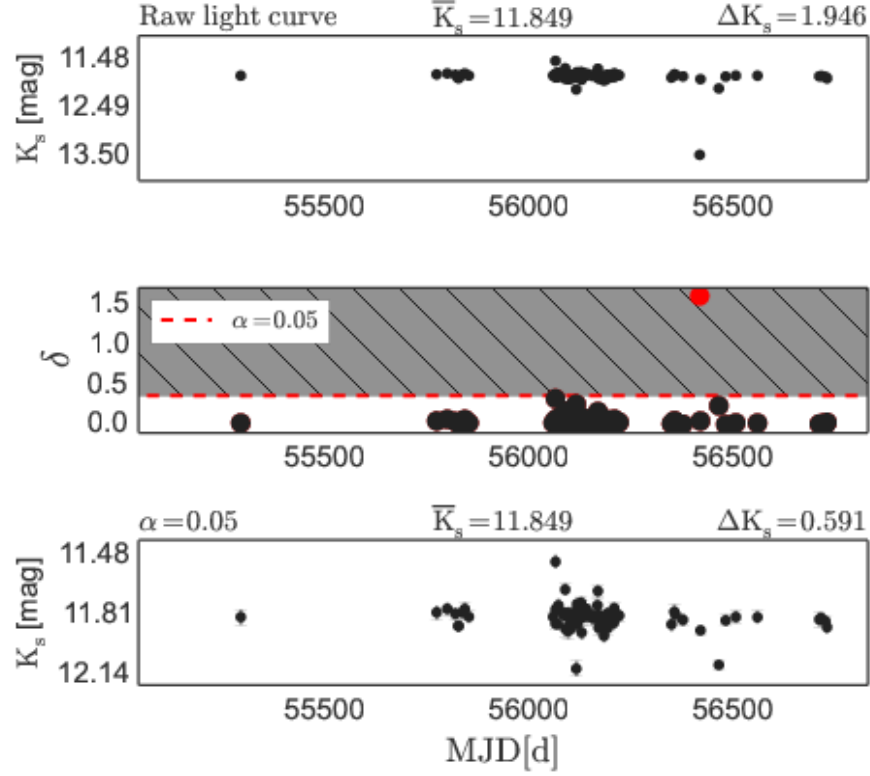


Figure 2. Performance of Thompson τ technique acting on a time series. Top plot: Raw light curve extracted from the photometric process. Middle plot: Absolute deviation δ of each measurements in function of MJD. The dashed red line indicates the rejection region (gray region) using $\alpha = 0.05$. The red point that fall in this region is removed from the sample. Lower plot: Modified time series, which will be used in the analysis.

In this work, we considered a set of six variability indices (see the references in Table 1) in order to characterize the behavior of the variable sources along time. Mainly, we used the amplitude ΔK_s and the η index to identify irregular variables. All these parameters are estimated directly from their K_s -band time series. All the procedures, and the automated process that we developed were summarize in the flux diagram of Figure 3.

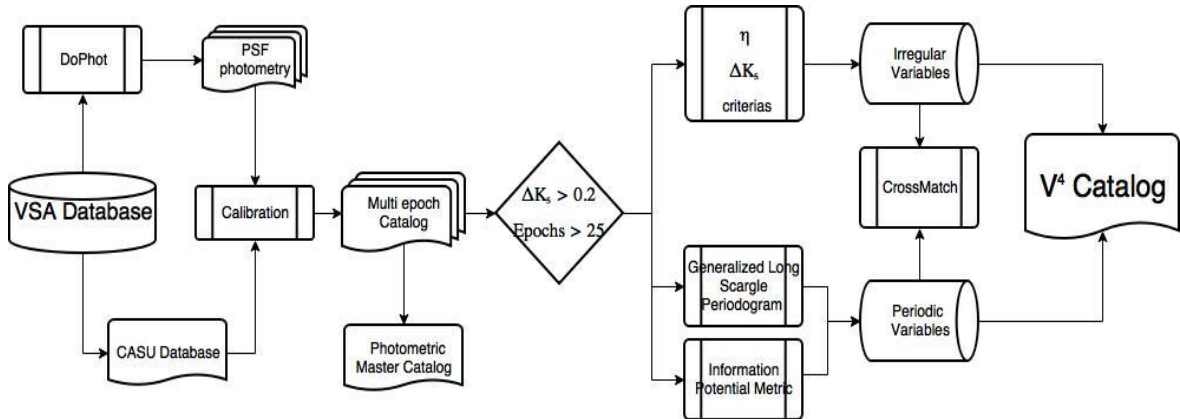


Figure 3. Schematic view of the automated process developed and used in this study to categorize the sources in the V^4 catalog.

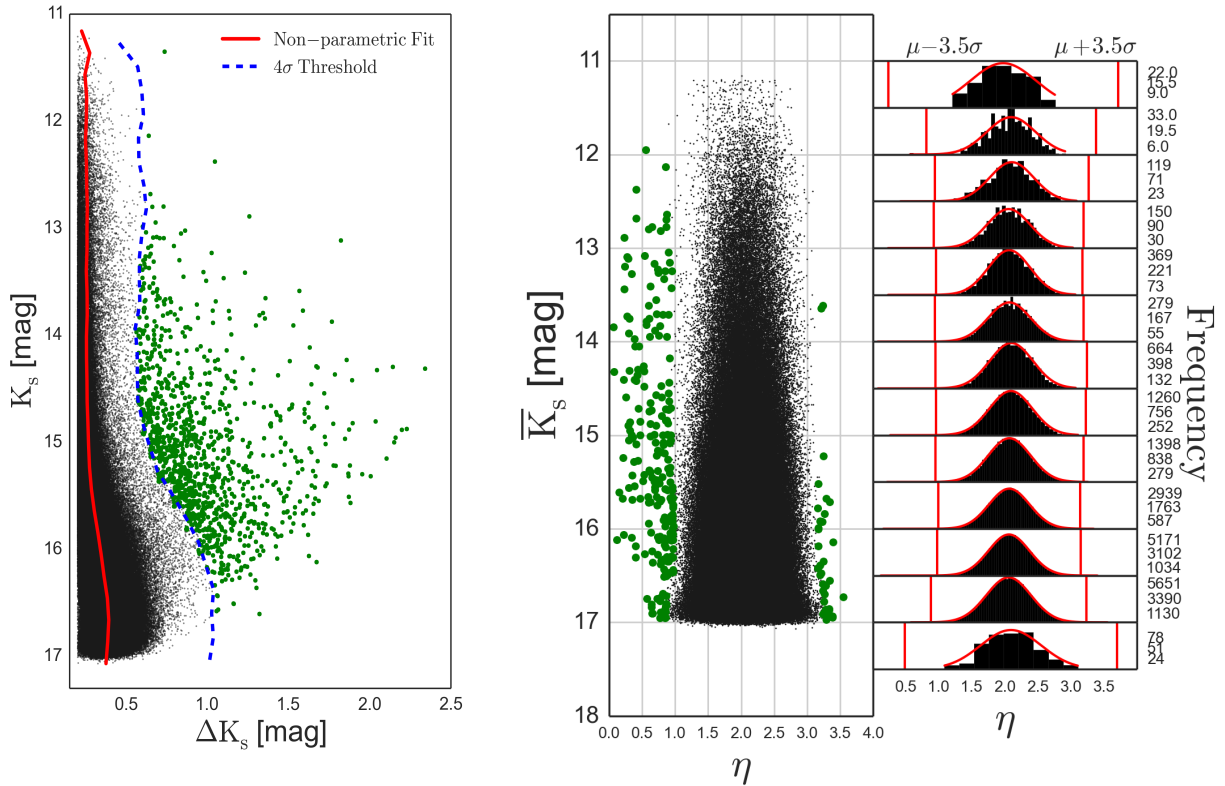


Figure 4. Representation of the two selection criteria aiming at identifying irregular variables. The dark points are all stars in the final photometric catalog, and the green filled circles highlight the selected sources by each method. Left panel: Total amplitude ΔK_s selection. The red solid line represent the non-parametric fit, while the dashed blue line displays for the 4σ threshold. Right panels: η index selection. The red lines in the bins of 0.5 mag represent the 3.5σ threshold of the Gaussian fit.

3.1. Identifying irregular variable sources

Eruptive Pre-main Sequence (PMS) stars are traditionally classified as FU Orionis Types (FUors, [Herbig 1966](#)) and EX Lupi (EXors, [Herbig 1989](#)) types. Their variations occasionally have high amplitudes (up to 2-6 magnitudes in optical bands) in a short time scales. Different physical processes have been proposed to explain the variations of these objects: accretion or variable extinction induced by their circumstellar disks, among others. These high amplitude variables are potential tracers of new generation of stars, so we expect to detect them within and close to the star forming regions (SFR) of the Galaxy.

As an example, in [Contreras Peña et al. \(2017a\)](#), the total amplitude ΔK_s was used as a discriminant to identify variable sources with $\Delta K_s > 1$ magnitude. This method was very useful to help identify likely YSOs amongst irregular and periodic variables stars projected against SFRs. The “Amplitude index” also performs satisfactorily in identifying sources with a large amplitude ΔK_s , like some Eclipsing Binary systems and likely pulsating asymptotic giant branch (AGB) stars as Miras and semi-regulars sources, which has periods longer than $P \geq 100$ days, and frequently are grouped under the name “long period variables” (LPV).

Following the same idea, we made a non-parametric fit on our photometric catalogs of d001 and d002. In order to quantify the behavior of ΔK_s as a function of mean magnitude \bar{K}_s , we measured the dispersion **in bins**, and selected those above 4σ . This allowed us to define dynamical thresholds, taking into account that the estimated σ depends on the stellar population projected on the different tiles (for example a tile containing a projected star forming region will have a different threshold assigned, than a tile with Population II stars). The left side of Figure 4 shows the amplitude ΔK_s selection for the sources found in tile d001.

To complement the previously described criterion, we performed an additional selection using the η index (von Neumann 1941; Shin et al. 2009; Sokolovsky et al. 2017). This statistic is defined as the squared addition of successive differences between adjacent observations in a time series:

$$\eta = \frac{1}{(N-1)\sigma_{ts}^2} \sum_{i=1}^{N-1} (m_{i+1} - m_i)^2, \quad (2)$$

where m_i are magnitude measurements, N the available number of epochs. The properties of the η index are well known for a stationary Gaussian distribution, but not for astronomical time series, because usually, they have an unequal sampling. For time series with uncorrelated photometric measurements (i.e. time series with an uncorrelated normally distributed measurements), the η index would have a value ~ 2 , and extreme values for series with long time variability trends. Given the aforementioned properties and the volume of the data, we expect that index η has a Gaussian distribution centered in $\eta \approx 2$. We separated \bar{K}_s into 0.5 magnitudes bins and considered 3.5σ confidence intervals on every bin to identify variable sources. The right two panels of Figure 4 show the η selection, and the fit of Gaussian functions in each histogram generated by separating the distribution in bins of 0.5 mag.

Each irregular variable should satisfy both $\Delta K_s, \eta$ criteria in order to be included in the paper as an irregular variable. All selected candidates have visual confirmation on the corresponding images, the candidates with close (less than 0.4 arcsec) companions are removed.

3.2. Identifying periodic variables stars

One of the main goals of the VVV Survey is to obtain a complete census of pulsating stars, such as RR Lyrae, Cepheids, Semi-Regular and Mira variables across the Milky Way. These sources provide useful information in their quality as standard candles (using the developed Period-Luminosity relations in the near-IR), to determine the structure of our Galaxy. These stars are also useful to map the extinction affecting the projected areas. Another potential set of targets to be identified are the Eclipsing Binary (EBs) systems, which are known to provide the most robust/model free estimates of the fundamental stellar parameters.

In this study, we have implemented two methods to identify periodic sources within VVV data:

- The Generalized Lomb-Scargle Periodogram (GLS, Zechmeister & Kürster 2009): A least-squares spectral analysis method based on the classical Lomb-Scargle Periodogram (Lomb 1976; Scargle 1982). In particular, we used its implementation in the `astroML`³ python library (Vanderplas et al. 2012)
- The Informatic Potential Metric Q_m (IP metric, Huijse et al. 2011): A discriminant designed to identify the fundamental period of a time series using information theory. Within this framework, different set of time series $\{x_n\}$ are assumed to be realizations of a continuous random variable X . The Informatic Potential is defined as follows:

$$\text{IP}_X(\{x_n\}) = \frac{1}{N^2} \frac{1}{\sqrt{2\pi}\sigma} \sum_{i=1}^N \sum_{j=1}^N \exp\left(-\frac{\|x_i - x_j\|^2}{2\sigma^2}\right). \quad (3)$$

We used a grid of trial periods P_t to fold the time series into phase space. The folded light curves are then segmented in H bins and IP is computed for every bin (h). The IP metric Q_m is computed as the squared differences between the information potential of each bin and the global IP:

$$Q_m(P_t) = \frac{1}{H} \sum_{h=1}^H [\text{IP}_X(\{x_n\}) - \text{IP}_X(\{x_n\}_{n \in h})]^2. \quad (4)$$

To estimate the reliability of the periods found with both approaches, we calculated the statistical significance for the spectral power peaks in GLS and IP metric. Only objects with peak-significance greater than 99.9%, were considered for further analysis and characterization. We note that this formal peak-significance assumes the uncertainties are described by uncorrelated Gaussian noise.

³ <http://www.astroml.org/>

3.3. Classification of periodic stars

To determine the variability type of the identified periodic stars, we consider the shape of the light curve, and the period P determined by the methods previously described. A common tool to quantify the shape of a light curve is using templates, where the light curves of periodic sources are compared with templates to assign a well define variability class, using one or a set of statistics to relying this classification. These templates could be collected from public archives, literature and other databases, in order to create “training sets” that points to an automated classification. In this context, a significant (and still increasing) number of infrared light curves templates have been assembled in the VVV Templates Project (Angeloni et al. 2014), where the main goal is to develop and test machine-learning algorithms for the automatic classification of VVV light curves. Nevertheless, we need to consider that in the NIR, RR Lyrae stars are a special case, given that the amplitudes of light curves decreases from optical to infrared wavelengths, this leads to being more difficult to differentiate between RR Lyraes in fundamental-mode (RRab) and first-overtone (RRc) subtypes using only Templates. In this context, we used two criterion to classify these periodic sources:

3.3.1. Using the VVV template project

We expect low accuracies in the period estimation due to the relatively small number of epochs, as we pointed out in section 2.2. With this in mind, we have used templates of those variables that we expected to find in this galactic longitude, such as Classic Cepheids and Eclipsing variables. The δ Scuti stars were not considered in this analysis given that just two light curve templates are available in K_s -band. Nevertheless, their periods are less than 0.2 days, and may have similar characteristics to EBs (Dong et al. 2017). Several δ Scuti sources were identified around open clusters in K_s -band (Palma et al. 2016), so we need more information for a well characterization of this type of variables.

We used templates of Classic Cepheid (103 templates in K_s , with $0.97 < P < 133.90$) and Eclipsing Binaries (76 templates in K_s , with $0.305 < P < 16.092$) to compare with light curves of our objects when its period P is contained in the indicated period range of the templates. To quantify these comparisons, we performed a Fourier fit of N harmonics into the phase space for each template and variable, given its period P and average magnitude $\langle m \rangle$ (see Figure 5). The amplitude A_k and the phase ϕ_k for each k harmonic were determined. The Fourier series $f(t)$ at time t is given by:

$$f(t) = \langle m \rangle + \sum_{k=1}^N A_k \sin \left(\frac{2\pi kt}{P} + \phi_k \right). \quad (5)$$

Each “synthesized” template was then normalized subtracting the integral of the obtained Fourier series. The harmonic number N used to fit the model to periodic sources is $N = 4$. The periodic stars are classified using the template that had the best goodness of the fit, using the reduced χ_{red}^2 statistics as the criterion. If a source has $\chi_{\text{red}}^2 > 1$, will remain as not classified.

3.3.2. Classifying RR Lyrae stars

RR Lyrae stars can be sub-classified by their locations in the Bailey diagram (Bailey 1902), given that RRc sources have shorter periods than RRab type. Figure 5 of Gavrilchenko et al. (2014) shows that RRab and RRc categories are located in different places of Bailey diagram. They also discuss the arbitrary limit $P = 0.4$ days to discriminate between these categories. Using this, we define the RRc region ($0.2 < P < 0.4$ days) and the RRab region ($0.4 < P < 1$ days), and they are shown in Figure 8.

4. APPLICATION OF THE AUTOMATED PROCESS ON D001 AND D002 VVV TILES: THE V^4 CATALOG.

4.1. Irregular variable sources

We had identified 72 variable sources that fulfill both the ΔK_s and η criteria. If a source presents periodicity, it is removed from the sample and add to the periodic sample. This was the case of two sources (d001-79, d002-103) which present a large amplitude and period, typical signatures of dust-enshrouded AGB stars, invisible in the optical range, due to its thick circumstellar envelope, a product of its high mass-loss rate.

Finally, we identified 70 irregular variable sources, 45 of them belonging to d001 and 25 to d002. Almost two thirds of them (64.28%) are projected in d001 tile and follow the cold gas/dust distribution as traced by the W3 ($\lambda_{\text{eff}} = 12\mu\text{m}$) band WISE image (the background of Figure 6). The highest over-density is observed at the borders of the star forming region, where the nebulosity is overwhelming, thus suggesting active star formation. All objects in the sample are, to the best of our knowledge, reported here for the first time. Some of these sources are shown in the Figure 7.

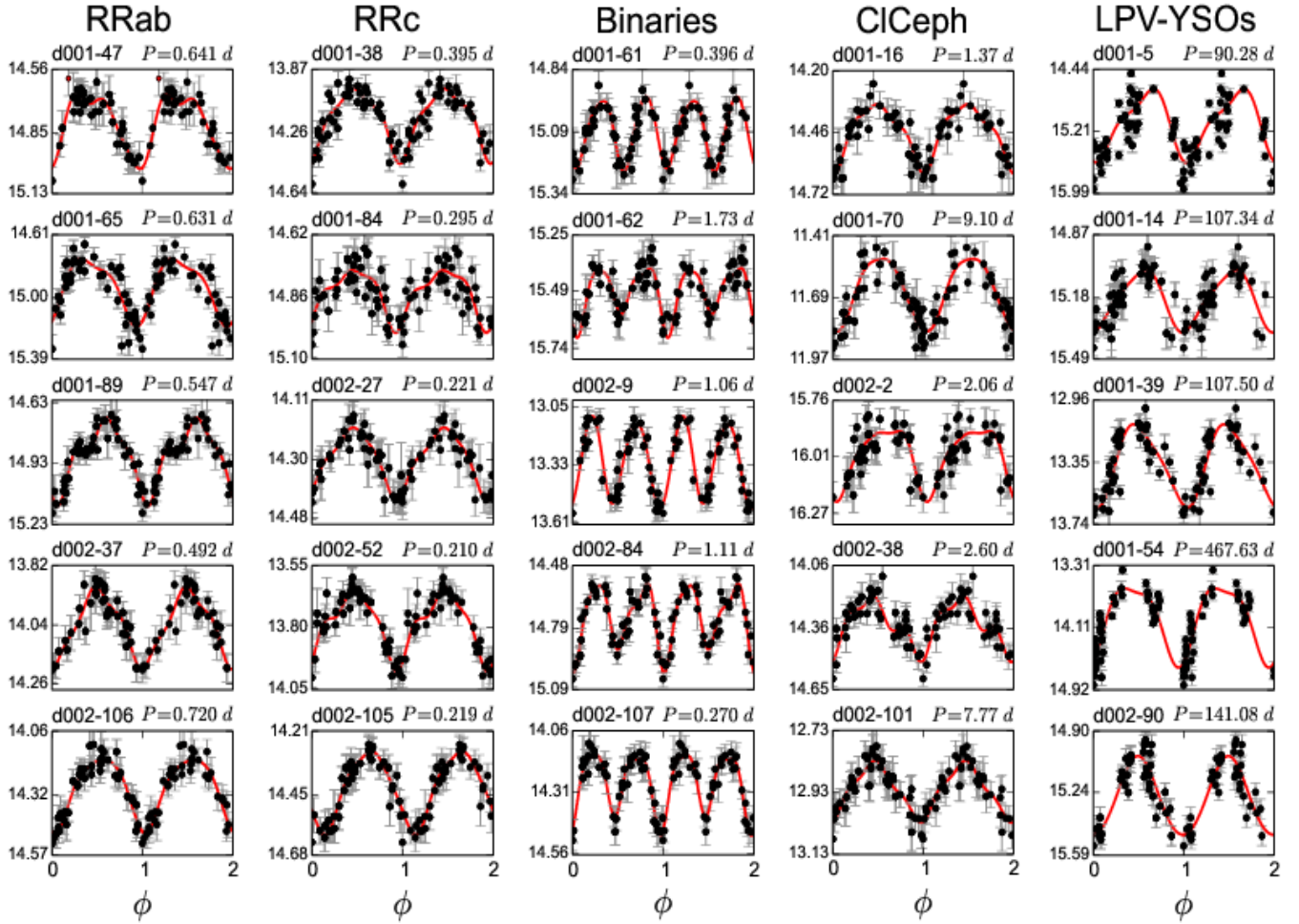


Figure 5. Examples of light curves of the periodic stars of RRab, RRc, Cepheid, Binary and LPV types. Red points in the phase diagram are outliers of the Fourier fit. In the top of each plot the identification ID and obtained period P are shown.

The sample can be separated in two groups:

- Short-term irregular sources: As discussed in 2.2, the cadence of VVV can reveal objects with large changes in their magnitudes in short periods of time, often associated with YSOs or PMS stars. Examples of such time series are shown in Figure 7. As noted previously, intrinsic changes in the sources can be explained by variable accretion (see e.g. Meyer et al. 1997; Rebull et al. 2014; Cody et al. 2014) referred to as bursts if there is a brief, well defined event and then a return to quiescence. Variable extinction is also possible. The individual characterization of the objects is beyond the scope of this paper, and they will be analyzed in an up-coming work, once the follow-up spectroscopic analysis is completed.
- Long-term irregular variables: This kind of sources have a slow change of their magnitudes over the time series, reaching large amplitudes ΔK_s in longer time intervals. In general, the sources do not exhibit large amplitude changes in short time intervals, but increasing/decreasing their luminosities monotonically, and then in certain cases returning to their mean magnitude. Possible mechanisms here are the eruptive episodes or long-term extinction events, followed by quiescent periods. These time series can also reveal stellar sources as supernovae, microlensing events (Minniti et al. 2015), LPVs, aperiodic long-term variability objects, and even extragalactic variable sources such quasars. Examples of long-term irregular time series can be seen on the right panels of figure 7.

In order to analyze the morphological behavior of VVV Irregular variable sources, Contreras Peña et al. (2017a), influenced by previous works such as Findeisen et al. (2013), proposed the following classifications for their sample of

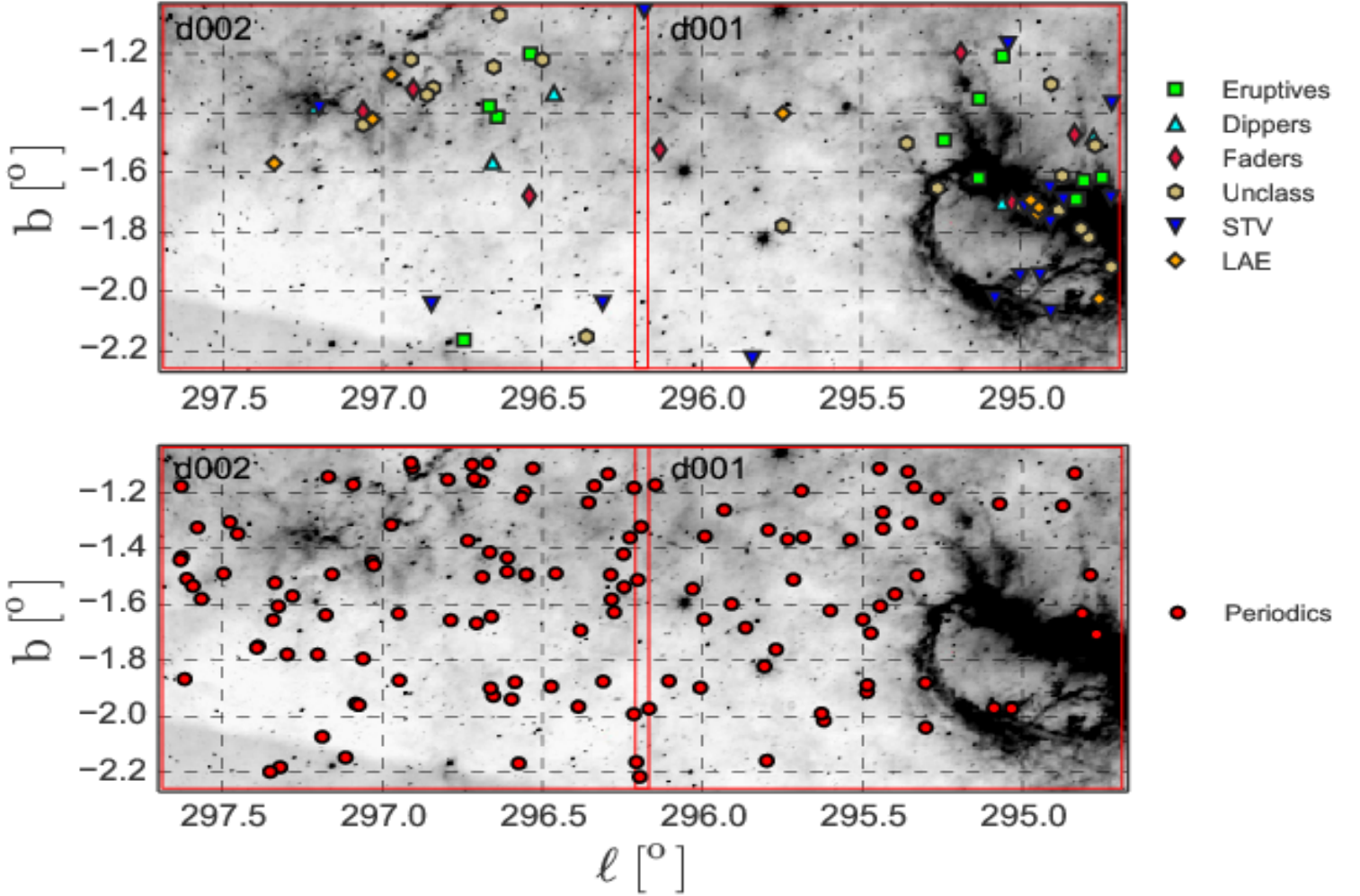


Figure 6. Covered region by d001 and d002 tiles from VVV survey, showing the spatial distribution of identified sources. Galactic north is up, galactic east is to the left. The symbols represent different types of variable stars found in the FoV, and are explained in Section 4. In background, W3 ($\lambda_{\text{eff}} = 12\mu\text{m}$) band WISE image is shown to illustrate the cold gas/dust distribution in the FoV.

high amplitude variables ($\Delta K_s > 1$ mag): Faders, Dippers, Short Time-scale Variables (STV) and Eruptives. However, half of our irregular variables sample has an amplitude $\Delta K_s < 1$ mag (right side of figure 9). Similar variable sources with low amplitude have been reported in literature (see for example Wolk et al. (2013) and Carpenter et al. (2001)) with light curves similar to those reported in this work. Therefore, given that classification for irregular variables is defined mainly by the shape of the time series, we extended the classification proposed in Contreras Peña et al. (2017a) for low amplitude sources ($\Delta K_s < 1$ mag), making an exception with the Eruptive classification, which describes sources with eruptions on timescales of hours to days. Sources that present eruptive long-timescales variability ($t > 1$ year) and $\Delta K_s < 1$ mag, will be classified as 'Low Amplitude Eruptive' (LAE). We used this classification to characterize our sources, when applicable. In Table 2, the main characteristics of the different proposed classes are explained.

4.2. Periodic variables stars

Our automated tool detected 22 periodic variable sources by the generalised Lomb-Scargle periodogram (GLS) analysis, both in d001 and d002 tiles, with range of periods between $4.03 < P < 1400$ days. Given the cadence of our data, and the limitations of the GLS, we can not obtain reliable periods shorter than 2 days. The IP metric, on the other hand, shows a great performance identifying periodic sources over the entire range of periods. Several stars have been detected by both methods, showing practically identical periods within the uncertainties. Thus, taking into

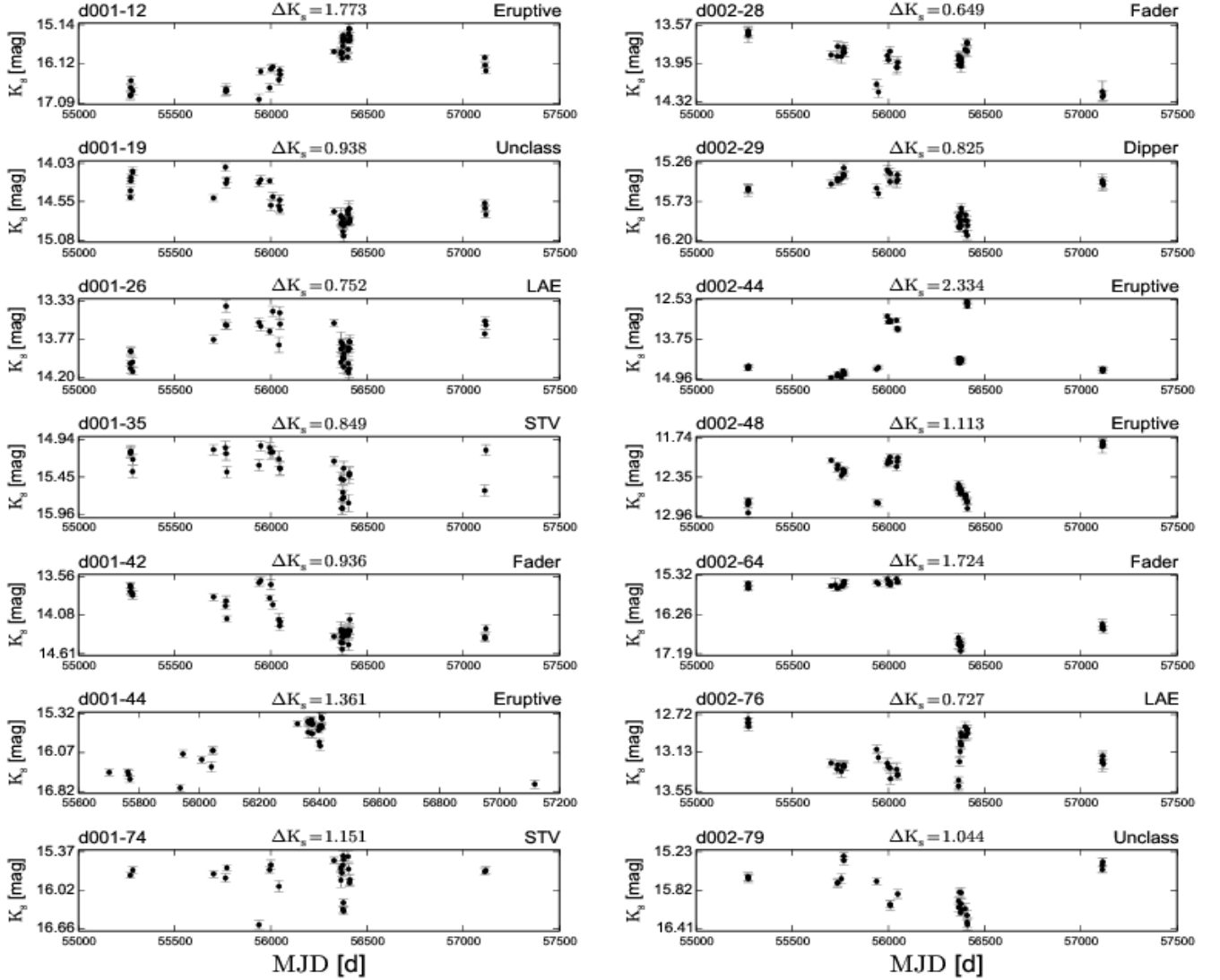


Figure 7. Examples of K_s -band time series of irregular variables. In the top of each plot the identification ID, mean magnitude \bar{K}_s , amplitude ΔK_s and variable type are shown.

account that the IP metric is computationally expensive, we used this method to search for shorter periods creating a grid of periods between 0.05 and 5 days. The IP metric identified 108 sources with $0.2 < P < 3.1$ days.

Figure 5 shows examples of the periodic variables, while in Figure 8 we show the Period-Amplitude diagram. As can be seen, most of the stars have short periods, typical for RR Lyrae stars.

In some cases it was not possible to distinguish between different variability types. For example LPVs and YSOs (Figure 5), thus we put mixed classification LPV-YSO, working on additional (spectroscopic) data to clarify.

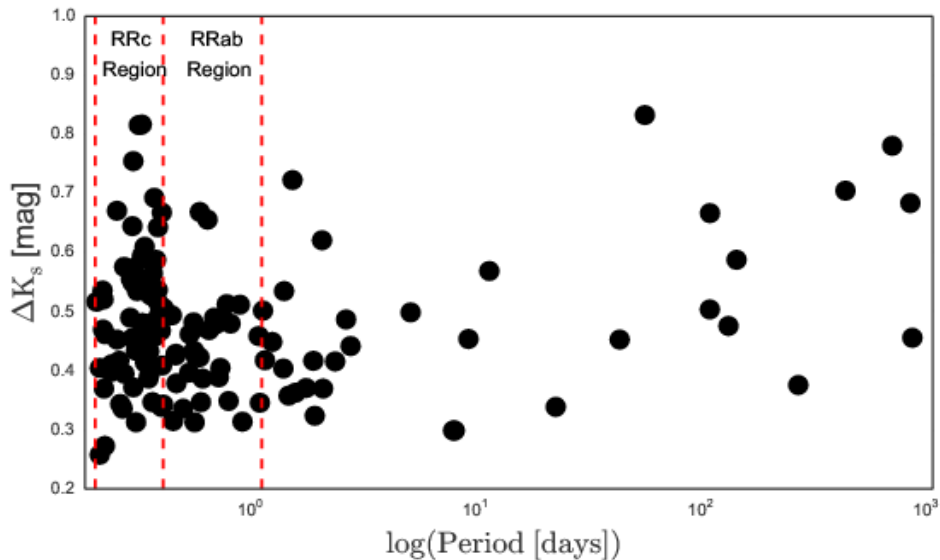
4.3. General properties of selected sources

Figure 9 shows the ΔK_s distribution of the selected sources as a function of the mean \bar{K}_s magnitude. The amplitude interval is between $0.5 < \Delta K_s < 3.2$ mag an average value of $\langle \Delta K_s \rangle = 1.1$ mag. The histogram is influenced mainly by the periodic sources.

Figure 10 shows the position of the variable stars in the color-magnitude and color-color diagrams. To plot the non-variable stars we used the first epoch of J and H band tile images taken in 2010. To analyze this, we have followed the method, described in Ojha et al. (2004). Three regions are defined: The 'F' region, which is located between the reddening vectors of giant and dwarf stars. The 'T' region is between the reddening vector of giant stars and CTTs

Table 2. Characterization of the irregular variables in the categories proposed by Contreras Peña et al. (2017a)

Class	Description
Dippers	Shows fading events, to then return to their normal magnitude.
Eruptives	Shows sources with outbursts with amplitude > 1 mag and duration longer than a few days and typically at least a year.
Low Amplitude Eruptive	Sources that present outbursts with amplitude lower than 1 mag and duration typically longer than a year
LPV-YSOs	Sources with a measured period, but with short-timescale scatter in the time series.
Short Timescale Variables	Sources with fast and constant scatter in their time series. They also can show brief rises in the magnitude in time scales of weeks.
Faders	Shows a continuous decrease in brightness ($t > 1$ yrs), or a big decrease in its brightness in a source with relatively constant luminosity.

**Figure 8.** Period - Amplitude diagram of periodic variables in our catalog.

locus, where the Class II YSOs objects and Herbig Ae/Be stars (Hillenbrand et al. 1992) can be identified. In the so-called 'P' region, located below the reddening vector of CTTS the likely proto-stellar objects are situated. Thus, the corresponding variability types are assigned. Column 32 of Table 5 contains the information of region in color-color diagram for each source.

4.4. The completeness and accuracy of the catalog

The catalog is limited to sources brighter than $K_s = 11$ mag, given the saturation of limit of VVV. We are only sensitive to the stars fainter than this magnitude limit. In the International Variable Star Index Catalog⁴ (VSX) are listed 57 variables in d001 and 46 in d002 fainter than $K_s = 11$ mag. From these, 30 sources in d001 and 36 in d002 are identified in the photometry catalog, but all of them have a typical ΔK_s around 0.2-0.3 mag, which is close to our conservative amplitude limit described in 2.3. This range of amplitudes is relatively low in comparison

⁴ <https://www.aavso.org/vsx/index.php?view=search.top>

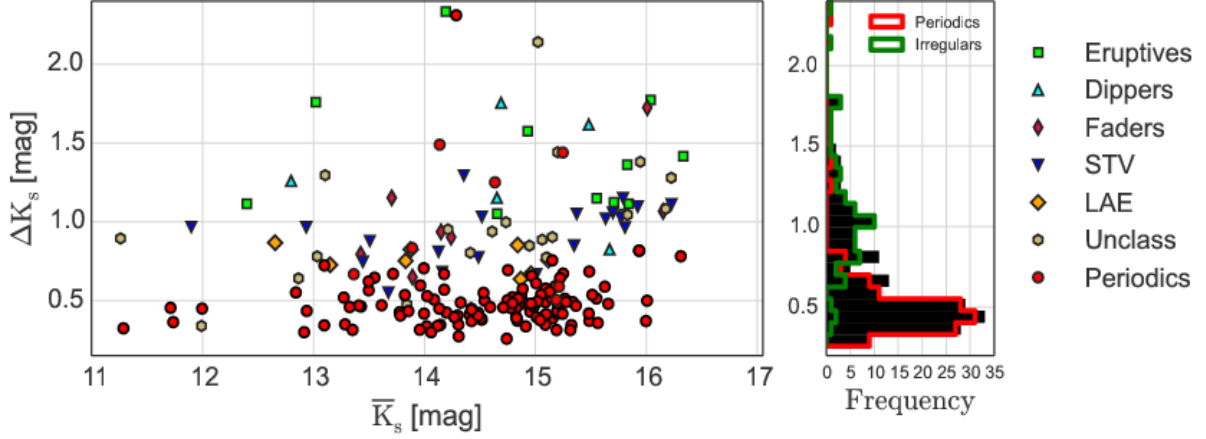


Figure 9. Left: The ΔK_s distribution of the selected sources vs. \bar{K}_s . Right: The histogram of ΔK_s distribution. In this figure, ΔK_s is truncated at 2.3 magnitudes, given that the source d001-79 has much larger amplitude than other sources ($\Delta K_s = 3.2$ mag). The symbols are the same as in the Figure 6.

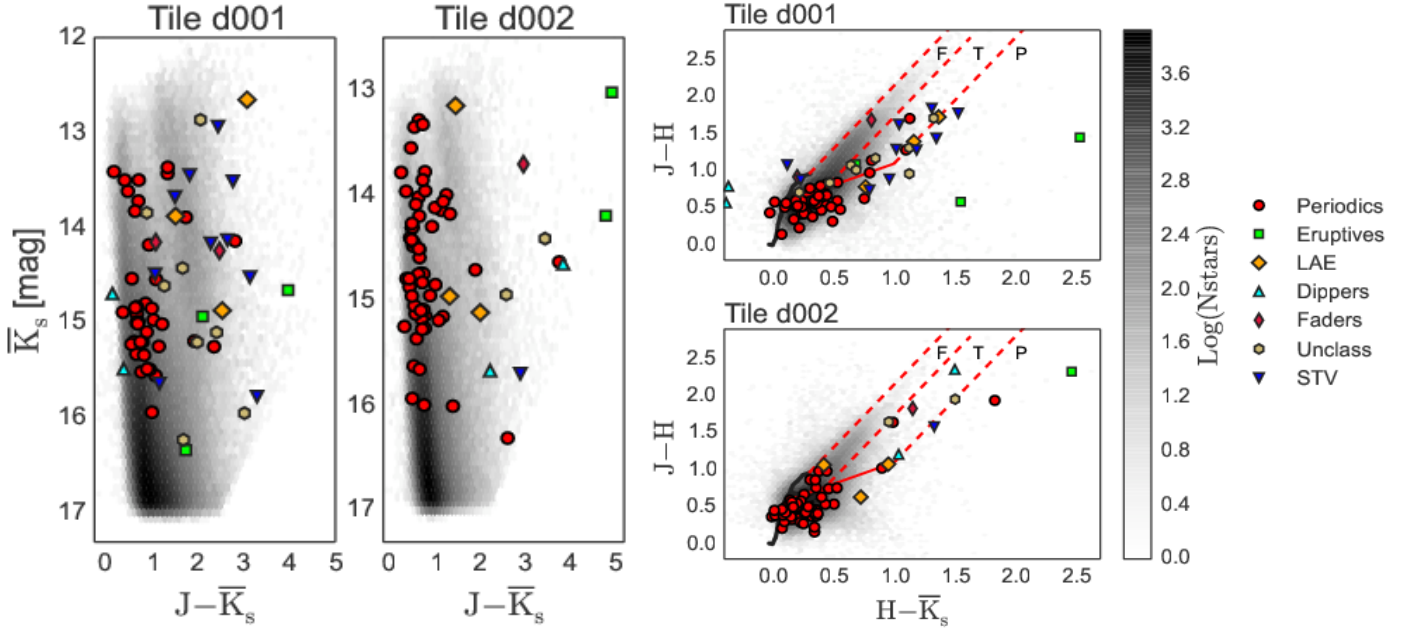


Figure 10. The color-magnitude and color-color diagrams of all variable stars in d001 and d002. The solid black lines are the intrinsic colors of dwarf and giants stars from [Bessell & Brett \(1988\)](#), the solid red line is the locus of un-reddened CTTs ([Meyer et al. 1997](#)), and the dashed red lines are the reddening vectors of the early spectral type dwarfs, giants stars and un-reddened CTTs, assuming a visual extinction $A_V = 15$ magnitudes. The symbols are the same as in the Figure 6.

of the average amplitude $\langle \Delta K_s \rangle = 1.1$ mag of the selected variable sources. (see figure 11). Taking into account that these variables are detected in the optical wavelengths, the amplitudes are too low to be detected in K_s -band with our searching method. Four sources from the VSX are recovered in our catalog, namely d001-20, d001-81, d002-8 and d002-60, the rest of the stars with amplitudes greater than 0.3 have least than 25 measurements. Thus, in the magnitude interval $11 < K_s < 15.5$ mag we recovered only 6% of the known optical variable stars, and more than 90% of our discoveries are new. In the context of previous K_s -band studies, [Minniti et al. \(2017\)](#) and [Eyheramendy et al. \(private communication\)](#) reported 1 and 13 RRab stars in d001 and d002, respectively. The [Minniti et al. \(2017\)](#) RR Lyrae star 'd002-0143595' has been re-discovered in our catalog as source d002-20, with practically the same period $P = 0.456794$ (with a discrepancy lower than 0.01%). Twelve of 13 RR Lyrae stars from [Eyheramendy et al.](#)

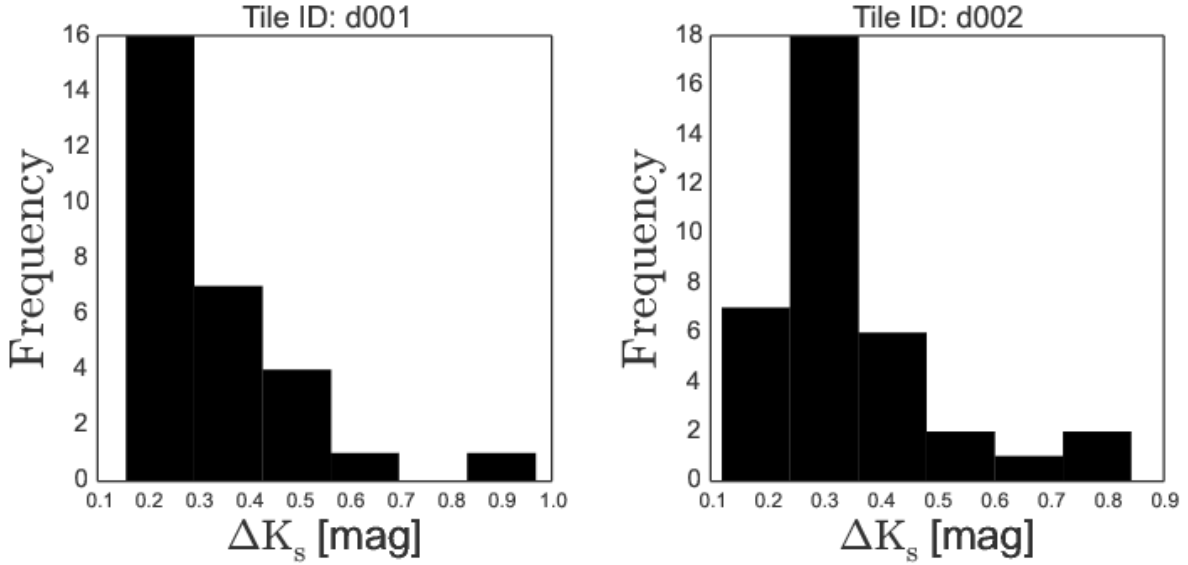


Figure 11. Histograms of the amplitudes of know variable stars from “International Variable Star Index Catalog” for d001 and d002.

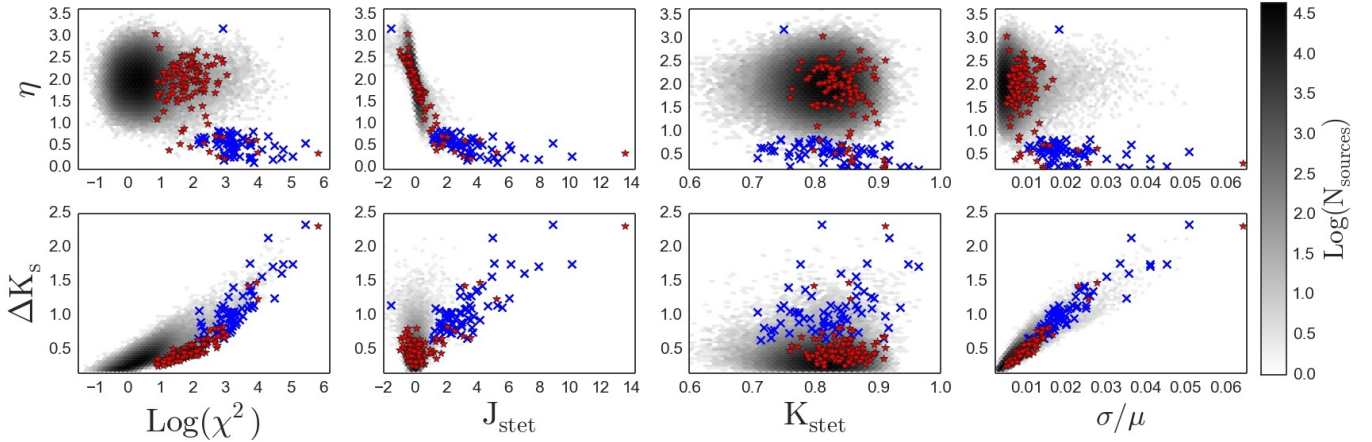


Figure 12. Correlation plots using the main features in this analysis. The blue crosses are the irregular variables, and the red stars are the periodic sources.

list are re-discovered in our catalog. The only source missed by our procedure has $\Delta K_s = 0.195$ mag and is rejected from our initial conditions. Thus, the completeness of the catalog $11 < K_s < 15.5$ mag is very close to 90%. We are expecting drops of the completeness for the fainter than $K_s > 15.5$ mag objects, but it is hard to estimate due to lack of literature data.

Figure 12 presents the main features η (top row) and ΔK_s (bottom row) as a function of different variability indices used in this article (see Table 1). The distribution of all detected sources in tile d001 is shown in background. The red stars represent the periodic sources, and the blue crosses are the irregular ones. As can be seen from the figure, the irregular variable sources are well separated from the distribution and follow different trends in the plots. The source d001-75 is an exceptional case, having an amplitude of $\Delta K_s = 1.151$ mag, $\eta = 3.193$, and a low number of observations (26 epochs). Excluding d001-75, the irregular sources fulfill $J_{\text{stet}} > 0.95$, which agrees with the limit used in [Rebull et al. \(2014\)](#). In the case of the periodic sources with short periods, in general they are located in the place where the main distribution is contained given the apparently uncorrelated shape of its time series, produced by the lack of observations.

4.5. Variable stars around open clusters in the d001 and d002 tiles

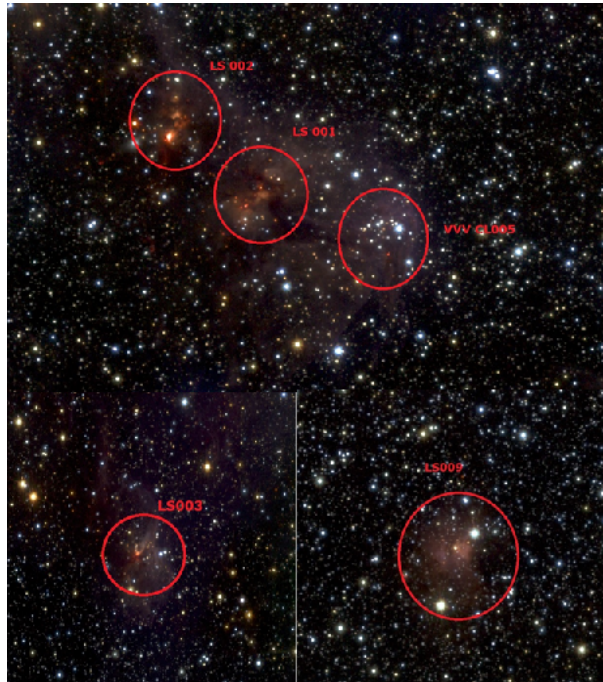


Figure 13. The false color VVV images of star clusters projected in d001. North is up, East is to the left. The red circles represent visual diameter of the clusters as defined in the text (see below).

Nine open cluster candidates are projected in the field of view of d001 and d002, namely VVV CL005, 007 and 009 (Borissova et al. 2011) and La Serena 001, 002, 003, 009 and 015 (Barbá et al. 2015). The coordinates of the clusters are listed in Table 3 and the VVV color images of clusters in d001 are shown in Figure 13 for illustration. Little is known about their properties, except for VVV CL009, which has been investigated in Chené et al. (2013) and Hervé et al. (2016). According to these papers, the VVV CL009 is young (4-6 Myr), moderately massive stellar cluster (total mass greater than $1000 M_{\odot}$), containing at least two O8-9V and an Oif/WN7 stars. The cluster distance of 5 kpc is estimated by Chené et al. (2013) using spectroscopic parallaxes. In the context of this paper, we search for variable YSOs around these clusters, that could be cluster members. To do this, we use the shape of the light curves, their position on the color-magnitude diagrams, the projection within the visual diameter of the clusters and proper motion diagrams taken from Smith et al. (2018).

To estimate the projected cluster radius, we combined the existing VVV K_s -band images (55 in case of d001 and 41 for d002 tiles) using the standard IRAF procedures and then, the PSF photometry with Daophot in IRAF was performed. The obtained magnitudes were transformed to 2MASS system using common stars. The details of these procedures can be seen in Borissova et al. (2011, 2014). These photometric catalogs were used to construct the stellar surface-density maps, by performing direct star counting in the K_s -band with a $5''$ bin radius, assuming spherical symmetry. The maps are normalized by the area of the rings to determine the stellar density. The resulting spatial distribution maps of the stellar surface density are shown in Figure 14.

As can be seen from Figure 14, the over-density of the stars is clearly visible, the density peaks are at least 3 times higher than the surface density of surrounding fields, thus confirming the cluster/group nature of the candidates. The cluster boundary was determined by fitting the theoretical profile presented in Elson et al. (1987). The obtained visual radii of the clusters are listed in Table 3, where the errors correspond to uncertainties from the model fit.

The procedure employed for determining the fundamental cluster parameters such as age, reddening, and distance is described in Borissova et al. (2011, 2014) and Chené et al. (2012, 2013). Briefly, to construct the color-magnitude diagram we perform PSF photometry of 5×5 arcmin J, H, and K_s fields surrounding the selected candidate, using the Dophot pipeline. Data for saturated stars (usually $K_s \leq 11.5$ mag, depending from the crowding) were replaced by

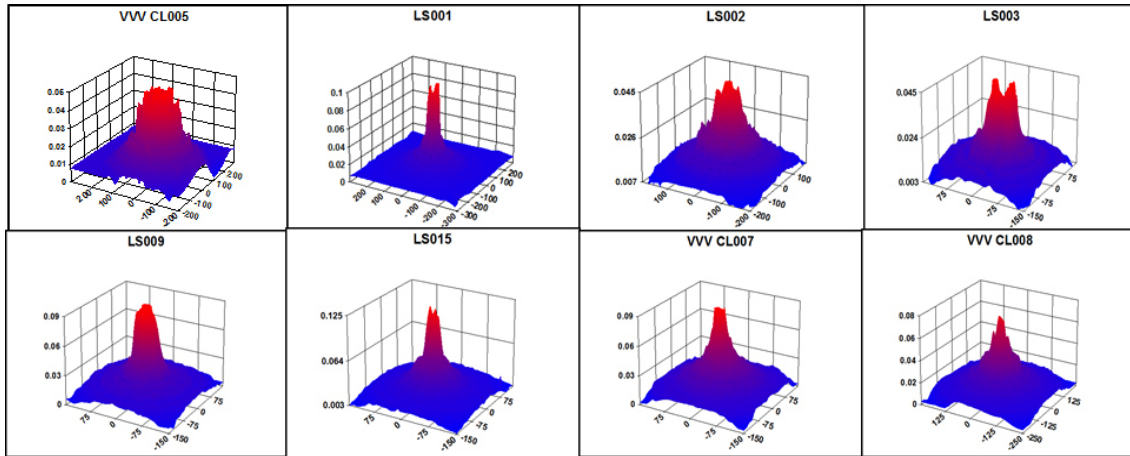


Figure 14. Stellar surface-density maps σ (stars/arcmin²) of the clusters.

Table 3. Basic information of the star cluster candidates in the region.

Tile ID	Name	Ra ₂₀₀₀ (h:m:s)	Dec ₂₀₀₀ (d:m:s)	ℓ (deg)	b (deg)	Radius (arcmin)	E(J – K) (mag)
d001	VVVCL005	11:38:59	-63:28:42	294.9481	-1.7353	0.50±0.15	1.4±0.3
	La Serena 001	11:39:13	-63:29:04	294.9726	-1.7292	0.52±0.10	2.8±0.6
	La Serena 002	11:39:22	-63:28:11	294.9896	-1.7188	0.52±0.17	3.1±0.4
	La Serena 003	11:40:28	-63:27:58	295.1026	-1.6779	0.48±0.09	3.2±0.5
	La Serena 009	11:45:04	-63:17:44	295.5571	-1.3788	0.72±0.10	2.2±0.3
d002	VVVCL007	11:53:50	-64:20:28	296.7463	-2.1629	0.33±0.08	2.2±0.2
	VVVCL008	11:55:29	-63:56:24	296.7611	-1.7328	0.42±0.10	1.4±0.2
	VVVCL009	11:56:03	-63:19:00	296.8331	-1.1105	0.60±0.20	1.0±0.1 ^a
	La Serena 015	11:55:23	-63:25:30	296.7131	-1.2336	0.33±0.07	1.4±0.2

a: [Chené et al. \(2013\)](#)

data from the 2 MASS Point Source Catalog ([Skrutskie et al. 2006](#)). Since 2MASS has a much lower angular resolution than VVV, when replacing stars we carefully examined each cluster to avoid contamination effects of crowding, using the Point Source Catalog Quality Flags available in 2MASS catalog.

To separate the field stars from probable cluster members we used the field-star decontamination algorithm of [Bonatto & Bica \(2010\)](#). The algorithm divides the K_s , $(H - K_s)$ and $(J - K_s)$ quantities into a grid of cells. For each cell, the algorithm estimated the expected number density of member stars by subtracting the respective field-star number density. Thus, each grid setup produced a total number of member stars N_{mem} . Repeating the above procedure for different setups, we obtained the average number of member stars. Each star was ranked according to the number of times it survived after all runs (survival frequency), and only the N_{mem} highest ranked stars were taken as cluster members. For the present cases we obtained survival frequencies higher than 85%. To additionally clean-up the diagrams, we used the relative proper motion catalog recently constructed by [Smith et al. \(2018\)](#). In general, the cluster members should form clearly visible overdensity with respect to field stars in the proper motion diagram. In our case (see Figure 15) it is impossible to separate the cluster members from the field stars, because the cluster members closely follow the motion of the Galactic disk. Nevertheless, they mark compact groups, slightly shifted from the disk population. To calculate the radius of the group, we started from the photometrically decontaminated candidates, calculated the mean proper motion and its error (quadratically adding to this error the mean of the

individual proper motion errors), and drew the circle with 3σ radius (blue circle in Figure 15). Thus, the stars with motion projected farther than 3σ from the circle are rejected.

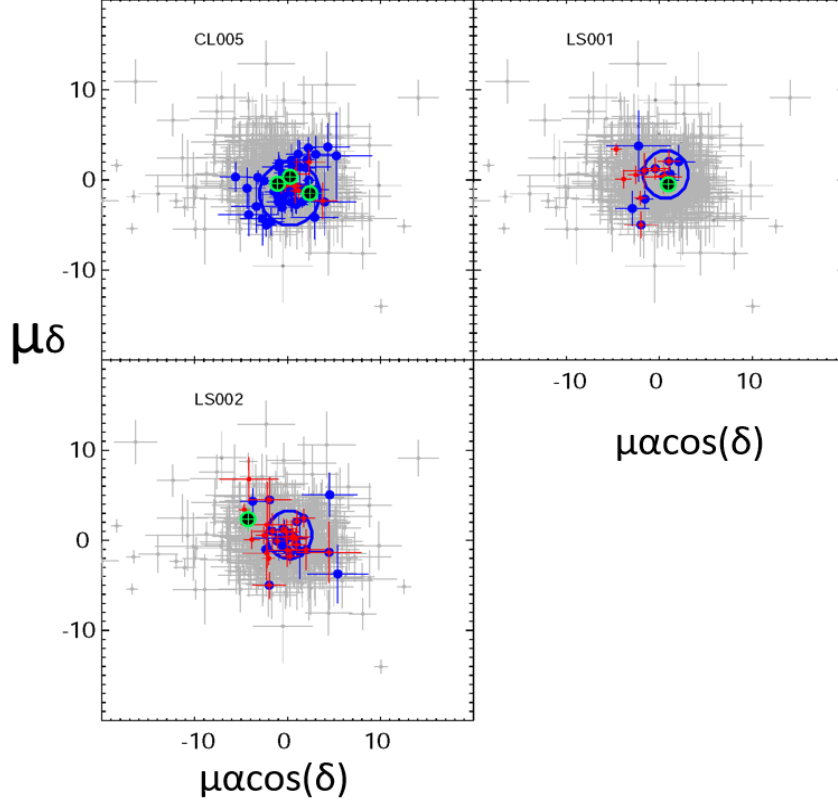


Figure 15. The relative proper motion of the CL005, LS001 and LS002. The gray points are all stars in 5x5 arcmin area, blue ones stand for most probable cluster members, obtained after statistical photometric decontamination procedure, red point are emission candidates (see text), and green ones are the variable stars. The big blue circle marks the suggested area of cluster members.

Taking into account that our candidates are classified as young clusters in the discovery papers of [Borissova et al. \(2011\)](#) and [Barbá et al. \(2015\)](#), the photometry/astrometry alone can not give accurate distance and age determinations. Usually, spectroscopic parallaxes from follow-up observations of selected members are needed. Here, only VVV CL005 has one follow-up object observed, thus it was impossible to obtain accurate basic parameters of the clusters. Instead, we use the PARSEC isochrones compilation for solar metallicity and ages of 5 and 400 Myr ([Bressan et al. 2012](#); [Marigo et al. 2017](#)) to illustrate the position of the most probable cluster members and to estimate their mean reddening (last column in Table 3).

4.5.1. Notes of individual clusters: VVV CL005

The cluster VVV CL005 is a young star cluster candidate, defined in [Borissova et al. \(2011\)](#) as a small group of 24 stars; it is projected close to the IC 2944 H II region and to the IC 2948 cluster (3.8 arcmin), on the part of the cloud [SMN83] Lam Cen 1. The brightest star within the cluster radius, namely HD308829, is classified as a Be star of B8 spectral type and is suggested to be a member of IC 2944 cluster (C1* IC 2944 THA 51). The star is found to be a periodic variable star with $P=0.8709$ days ([Pojmanski 1998](#)), but we can not follow its variability with VVV, because the star is saturated in our images ($K = 9.68$ mag). The published distance to the IC 2944 H II region varies from 1.8 kpc ([McSwain & Gies 2005](#)) to 2 kpc ([Sana et al. 2011](#)) in the literature. The color-magnitude diagram of VVV CL005 (Figure 16) shows a poorly populated main-sequence and some reddened stars, suggesting indeed a very

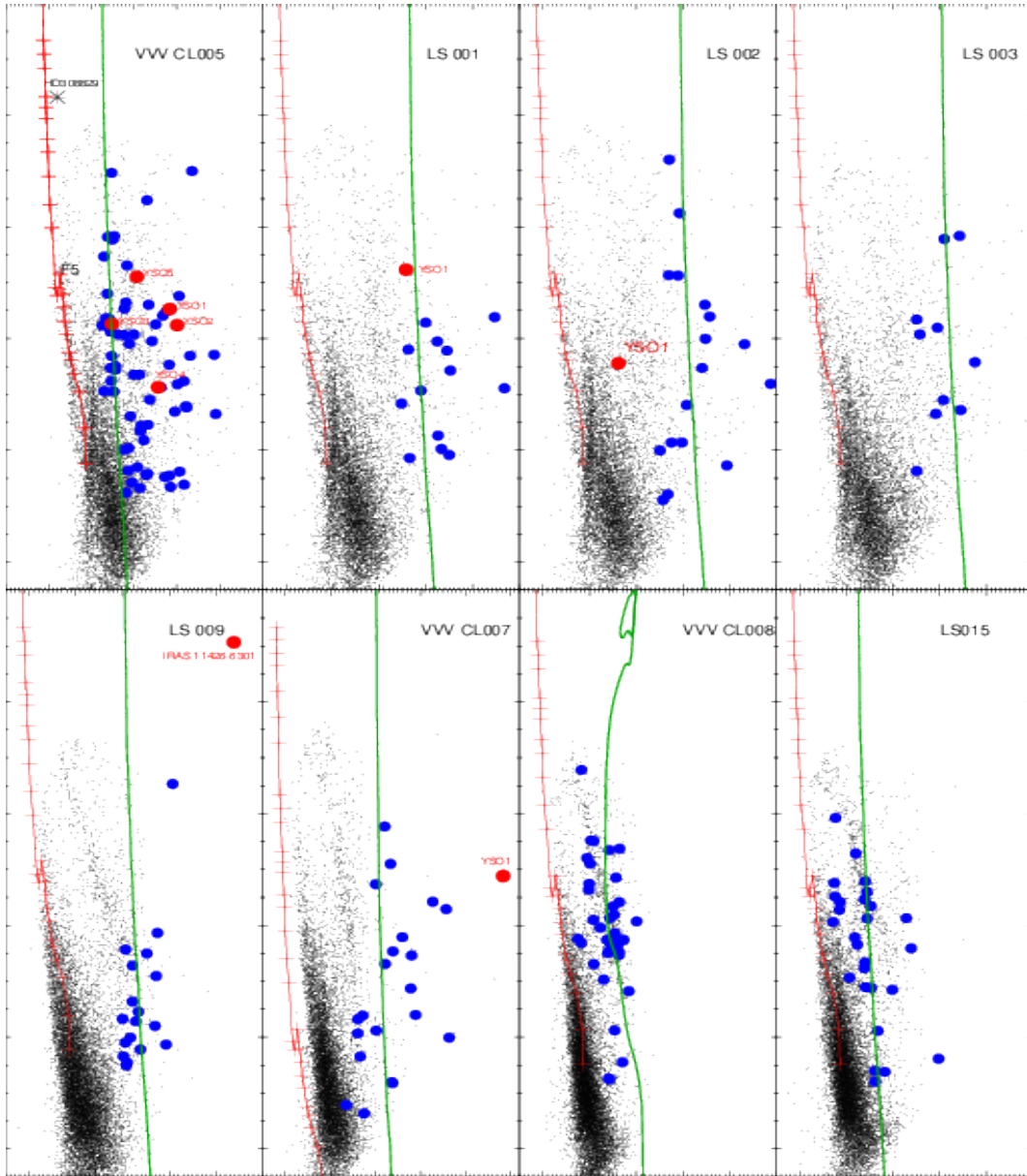


Figure 16. The K_S vs. $(J - K_S)$ color-magnitude diagrams for the clusters in the field of view of d001 and d002. Black points are all stars in 5×5 arcmin field around cluster centers, blue circles are the most probable cluster members, after statistical photometric decontamination. Red circles are variable stars (see text). The Geneva isochrones of 5 Myr (400 Myr for VVV CL008) and $Z=0.020$ are plotted with green lines. Red line represents the sequence of the zero-reddening stars of luminosity classes V (Schmidt-Kaler 1982) for illustration.

young stellar group. With regards to the distance, it is impossible to estimate it from comparison with the theoretical isochrones, because the isochrones for ages younger than 5 Myr in this mass interval in the near infrared bands are vertical and practically identical. Then, the spectroscopic distance is calculated using the spectral classification of Obj1 (Ra=11:38:57.73 and Dec=-63:28:22.4). The object is observed with the ARCoIRIS (Astronomy Research Cornell Infra Red Imaging Spectrograph). This is a cross-dispersed, single-object, longslit, infrared imaging spectrograph, mounted on Blanco 4-m Telescope, CTIO. The wavelength range is from 0.80 to 2.47 μm , with spectral resolving power about 3500. The comparison with different spectral templates taken from VOSA (Bayo et al. 2008) gives the most probable spectral type F4-F6V, used to estimate the spectroscopic parallax. We calculated reddening and distance modulus of $E(J - K_S) = 1.4 \pm 0.3$ and $(M - m)_0 = 10.45 \pm 0.43$ mag (1.23 ± 0.24 kpc), respectively. The distance

is comparable with distance estimates of 1 kpc as measured from the interstellar silicon monoxide (SiO) sources (Harju et al. 1998). Five variables (d001-25, 27, 28, 29, 30, see Table 6) are probable cluster members, taking into account their projected position radius from the cluster center and the position in the color-magnitude and proper motion diagrams (Figure 16, Figure 15). All of them show irregular variability, with relatively large amplitudes ($0.63 < \Delta K_s < 0.88$ mag) and thus can be classified as YSOs.

4.5.2. *La Serena 001*

The star cluster candidate La Serena 001 (LS001) is projected very close to VVV CL005, on the same H II region and contains a few very reddened stars (see Figure 16). These objects are deeply embedded in dust and gas. We adopted the same distance as for CL005, and using 5 Myr isochrone determine $E(J - K) = 2.8 \pm 0.6$. Note the large uncertainty of the reddening determination, which can be result of a strong differential reddening inside the region. One variable star (d001-32) is found in the vicinity of this group in formation. It shows an irregular time series and $\Delta K_s = 0.96$ mag. Taking into account the time series and its position of the CMD (in the 'P' region), most probably it is an YSO candidate.

4.5.3. *La Serena 002*

The star cluster candidate La Serena 002 (LS002) is projected close to LS001 in the North-East direction. Several embedded and very red sources are visible, indicating stars in formation. The color-magnitude diagram is poorly populated, thus as in the case of LS001 we determined the mean reddening of $E(J - K) = 3.1 \pm 0.4$ adopting the same distance modulus as above. One periodic variable star (d001-38) is found, with $\Delta K_s = 0.453$ mag and period $P = 42.706$ days, which we classified as a Cepheid. Additionally, this source is far from the main locus of most probable cluster members in the color-magnitude and proper motion diagrams, thus we conclude that is a projected field star. Two more irregular variables (d001-35, d001-36, see Table 6) with amplitudes between $0.84 < \Delta K_s < 0.91$ mag are most probably cluster members and YSO candidates.

4.5.4. *La Serena 003 and La Serena 009*

The star cluster candidates La Serena 003 and 009 are groups of stars in formation, deeply embedded in dust and gas. No stars with variation in the magnitude above our sensitivity limit of $\Delta K_s > 0.2$ mag are found in the vicinities of clusters. One YSO candidate IRAS 11426-6301 in the field of LS009 is reported by Kwok et al. (1997). Later on, Mottram et al. (2011) and Lumsden et al. (2013) resolved the source to YSO (G295.5570-01.3787A) and H II region (G295.5570-01.3787B, separated by 5 arcsec) on the base of far-infrared MSX measurements. They determined the radial velocity of 37.2 km/s and kinematic distance to both sources of 10.4 kpc. The bolometric luminosities of the YSO is calculated as $5980 L_\odot$, while the H II region has $63570 L_\odot$, the log Mass of the whole clump is estimated to be $3.106 M_\odot$ according to the same authors. Navarete et al. (2015) reported an extended H II emission associated with the region. Our K_s -band light-curve (Figure 17) shows low amplitude variability of 0.27 mag during the 2010-2015 time interval, with $\bar{K}_s = 11.365$ mag. Note, however that the 2MASS magnitude (taken from “The 2MASS Extended sources catalog” (Skrutskie et al. 2006)) is $K = 8.94$ magnitude, thus the star most probably shows a long-term variability.

IRAS 11426-6301 was observed on May 2017 with ARCoIRIS spectrograph, with 480 sec. integration time, at 1.28 average airmass. We reduced the spectrum using the `Spextool` IDL package (version 4.1, Cushing et al. (2004)), which is a data reduction algorithm specifically designed for the data format and characteristics of ARCoIRIS by Dr. Katelyn Allers. Telluric correction and flux calibration of the post-extraction spectra are achieved through the `xtellcorr` IDL package (Vacca et al. 2003). Figure 17 shows the spectrum, normalized at 2.293 microns. As can be seen from the figure, the continuum level is flat to slightly rising. The overall spectra energy distribution is peaking at around 2.5 microns. The H I and He I lines are clearly visible in absorption, some Ti lines and Na I doublet (2.21 microns) in absorption also can be identified. The Ca I triplet (2.26 microns) and ^{12}CO bands (2.29 microns) are missing. While the H I and He I represent in general early type stars, the Ti and Na features are typical of low mass YSOs. The absence of CO band means a absence of circumstellar disk. A possible explanation for this contradiction could be related to the photodissociation of CO molecule. This phenomenon (where one even detects CI but no CO, or a much lower abundance than expected) has been observed around young A-type stars in deep searches for molecular gas in debris disks (Higuchi et al. 2017). Thus, the spectrum shows mixed features arising from both high and low mass young stars. Taking into account the kinematic distance of 10 kpc this object could be an unresolved compact cluster or group of young stars.

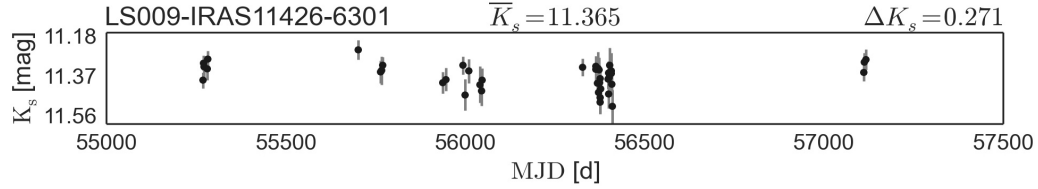


Figure 17. The VVV time series and the ARCoIRIS spectrum of IRAS 11426-6301 YSO candidate.

4.5.5. VVV CL007

One variable (d002-35) is detected with our algorithm very close to the center of VVV CL007 cluster. Taking into account its high amplitude $\Delta K_s = 1.76$ mag, its position on the CMD (in the 'P' region) and its classification as Eruptive variable (Contreras Peña et al. 2017a) most probably is it a YSO.

4.5.6. VVV CL008, VVV CL009 and La Serena 015

No variable stars are detected around VVV CL008, CL009 and La Serena 015. In Chené et al. (2013) we classify the Obj 4 (Ra=11:56:03.03 and Dec=-63:19:00.72) of VVV CL009 as a Be star.

In summary, only a few variable YSOs around the clusters are detected in the near infrared.

4.6. Stars with H α photometric emission

The clusters in the tile d001 are very young, still in formation and are surrounded by dust and gas, thus we can use the photometric catalogs from VPHAS+ survey (Drew et al. 2014) in order to search for additional YSOs and H α emission candidates. The VPHAS+ catalog contains magnitudes in five filters: u ($\lambda_{\text{eff}} = 354\text{nm}$), g ($\lambda_{\text{eff}} = 475\text{nm}$),

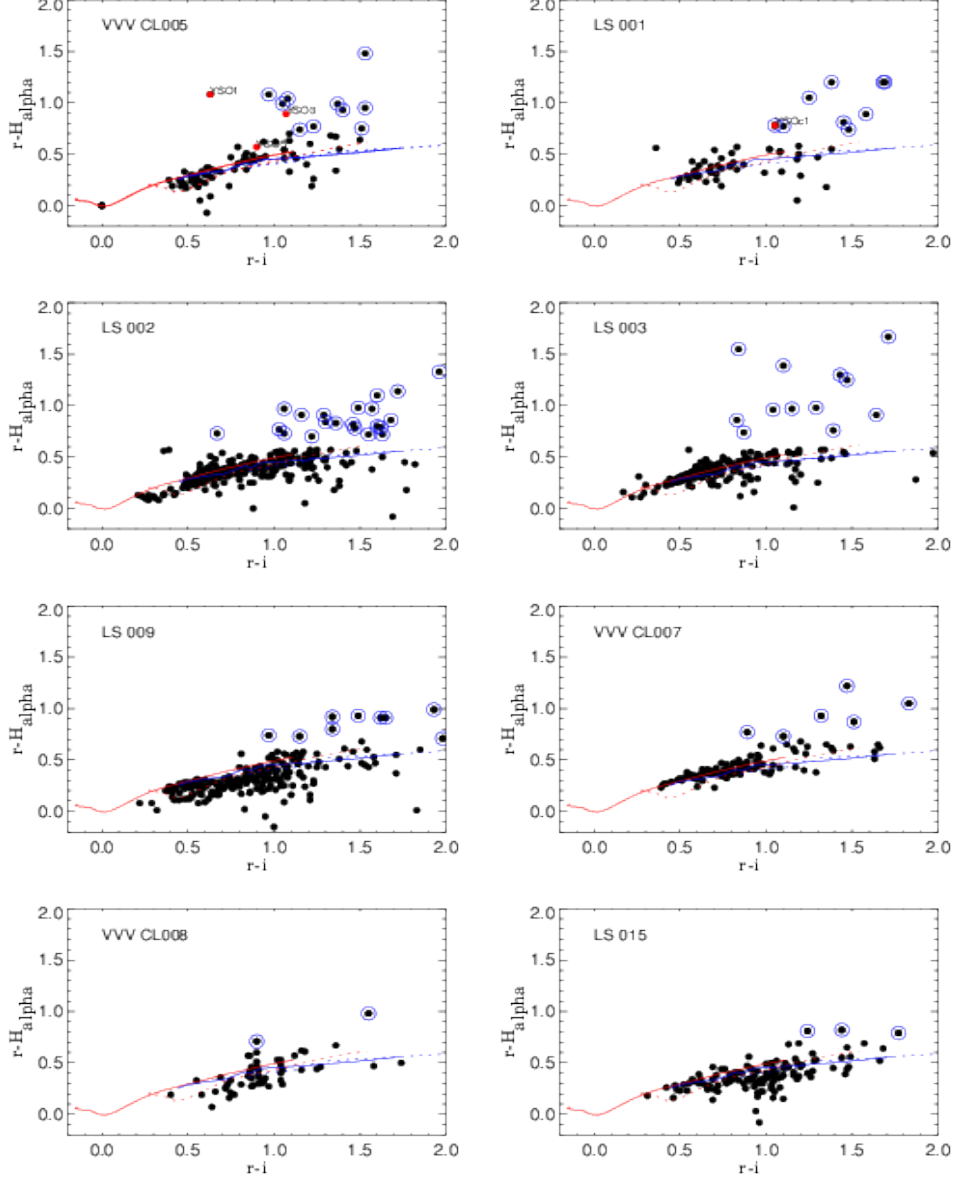


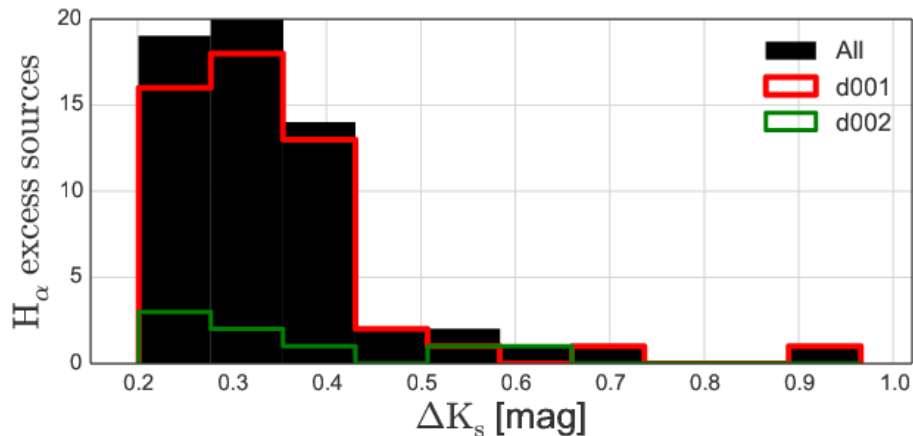
Figure 18. The $(r - H_{\alpha}, r - i)$ color-color diagrams. Blue circles show the selected emission stars, the red and blue solid lines are the synthetic unreddened main sequence and giant sequences, while the dashed ones corresponds to the corrected for the reddening sequences (Drew et al. 2014). Red circles in the top plots are infrared variable YSOs found in this work.

r ($\lambda_{\text{eff}} = 622\text{nm}$), i ($\lambda_{\text{eff}} = 763\text{nm}$) and H_{α} ($\lambda_{\text{eff}} = 659\text{nm}$). Following Kalari et al. (2015), we construct the $(r - i, r - H_{\alpha})$ color-color diagrams using DR2 of VPHAS+ catalog. The main-sequence stars do not show any H_{α} emission with respect to the r -band photospheric continuum. We use the VST/OmegaCAM synthetic colors for main-sequence and giant stars in the $(r - H_{\alpha}, r - i)$ plane (Drew et al. 2014) and selected the stars with more than 5σ deviation from these synthetic sequences, corrected for the corresponding reddening (dashed lines in Figure 18). The 73 selected sources are shown in Figure 18 and summarized in Table 4.

The cross-identification of these sources with the K_s variability catalogs shows that the peak of amplitudes is around 0.3 mag (Figure 19). As we stated in section 2.3, we set our detection limit of spread of the magnitude measurements with time to be greater than 0.2 mag. For sources below this threshold, we treat these objects as constant at our sensitivity level. Thus, only a few of the infrared variable YSOs (d001-25, d001-32) are emission line object candidates.

Table 4. VPHAS+ r , $(r - i)$ and $(r - H_\alpha)$ magnitudes and colors of the YSO candidates. The full version is available online.

ID	RA ₂₀₀₀	DEC ₂₀₀₀	r	$r - i$	$r - H_\alpha$
	(deg)	(deg)	(mag)	(mag)	(mag)
CL005 C1	174.71433	-63.48757	17.98±0.02	1.08 ±0.011	1.04 ±0.01
CL005 C2	174.71582	-63.46827	19.39±0.04	0.97 ±0.025	1.08 ±0.03
CL005 C3	174.71664	-63.48768	20.29±0.10	1.53 ±0.054	0.95 ±0.09
CL005 C4	174.71783	-63.48682	18.37±0.02	1.05 ±0.011	0.99 ±0.02
CL005 C5	174.71942	-63.4668	19.67±0.05	1.37 ±0.032	0.99 ±0.04

**Figure 19.** The distribution of amplitudes in the K_s -band of the emission line candidates.

5. SUMMARY

We have developed an automated process for identification, classification and analysis of variable sources using the VVV K_s -band time series, which are extracted directly from the 1.5×1.2 degrees image tiles. This process was created to automatically analyze the VVV tiles, given the huge amount of available data. The sources that present variability in the NIR are cataloged, in order to understand the physical process behind its variability, its spatial distribution, evolutionary state and relation with its environment. The gathered information from these sources will be collected in "VVV Variables (V^4)" catalog, which will be publicly available in VISTA Science Archive (VSA, <http://vsa.roe.ac.uk/index.html>) database and constantly updated adding newly processed VVV tiles.

This process is based on *Dophot* PSF photometry to create a multi-epoch K_s -band catalog of detected sources in the FoV. We also obtained the J and H band photometry, using the data taken in 2010. All the PSF photometry was calibrated using the aperture catalogs made by CASU. To test this method, we select d001 and d002 tile regions, covering an area of ~ 3.6 deg². A total of 1,308,626 point sources between $10.8 \leq \bar{K}_s \leq 17.2$ mag were detected. The time series of sources with more than 25 epochs and amplitude $\Delta K_s > 0.2$ mag were selected and analyzed through different methods in order to detect real variables. To avoid outliers, suspicious photometric measurements were removed from the light-curves using the modified Thompson τ technique.

Our automated tool identified 200 sources with prominent NIR variability. Using two main variability indices (ΔK_s , η), we identified 70 variable sources without periodic or semi-periodic behavior, which are bona-fide irregular variables. On the other hand, we used periodograms (GLS, IP) to identify periodic sources, finding 130 of them. All identified

sources have an average K_s magnitude distributed between $11.2 < \bar{K}_s < 16.4$ mag, and a total amplitude contained between $0.2 < \Delta K_s < 3.3$ mag. About 90% of these sources are previously unknown as variable stars.

For each source with available J and H photometric measurements, its position in the (H – K_s , J – H) color-color diagram was reported, dividing this diagram into three parts (the 'F', 'T' and 'P' region), following the procedures of Ojha et al. (2004), in order to extract information about the evolutionary state of those sources.

In the case of the irregular variable sources, they were classified using the framework of Contreras Peña et al. (2017a), who use the time series morphology to classify the sources into 5 categories (Dippers, Eruptives, LPV-YSOs, STVs, Faders). The LPV-YSO sources, together with the periodic variable sample, will be analyzed in a subsequent paper. Sources that could not be classified unambiguously into the aforementioned categories, are marked as "unclassified". In total, we classified 20 STVs, 12 Eruptives, 5 Dippers, 7 Faders, 8 Low Amplitude Eruptive Variables, and 18 sources remained unclassified. These variable stars have amplitudes $\Delta K_s > 0.63$ mag, $\eta < 0.82$ and $J_{stet} > 0.95$, without counting the source d001-75, which has $\eta = 3.193$. and $J_{stet} = -1.55$.

We examined some parameter distributions in the specific parameter space (Graczyk & Eyer 2010) in order to separate the variability types. For example a χ^2 parameter (in logarithmic scale) can separate the periodic sources from the main distribution when $\log(\chi^2) > 0.8$. In the future, we will use this to optimize the process of generation and analysis of time series and light curves in the VVV in the supervised algorithms of machine learning.

We classified 25 RRab, 42 RRc, 13 Classic Cepheids, 33 Binaries, 7 LPV, 7 LPV-YSOs and three periodic variables remain unclassified. The periodic sources have a distribution of periods between $0.2 < P < 1430$ days and an average K_s magnitude distributed between $11.3 < \bar{K}_s < 16.32$ mag.

We also analyzed nine open cluster candidates using surface-density maps, color-based decontamination and proper-motion decontamination algorithms to determine the radii of the clusters. We have estimated the mean reddening $E(J - K_s)$ by comparison with the PARSEC isochrones for solar metallicity. We were only able to determine a distance modulus for VVV CL005 cluster, using the spectroscopic parallax. This cluster also has the largest number of irregular variables as probable cluster members (d001-25, 27, 28, 29 and 30). The cluster LS002 has two irregular variables, while clusters LS001 and VVV CL007 have one irregular variable, each other, as probable cluster members. All irregular sources projected close to open clusters in the region are young stellar object candidates.

Given the low number of irregular variable sources that we found around open clusters, we used the VPHAS+ survey to identify excess in H_α -band. We have selected 73 stars with more than 5σ difference from the VST/OmegaCAM synthetic colors for main-sequence and giant stars in the ($r - i, r - H_\alpha$) plane (Drew et al. 2014). We noted that 64% of this sample has low amplitude $\Delta K_s < 0.4$ mag, so this could be a good complementary method to find YSOs.

6. ACKNOWLEDGMENTS

We gratefully acknowledge data from the ESO Public Survey program ID 179.B-2002 taken with the VISTA telescope, and products from the Cambridge Astronomical Survey Unit (CASU), also on data products from observations made with ESO Telescopes at the La Silla, Paranal Observatory under programme ID 177.D-3023, as part of the VST Photometric H_α Survey of the Southern Galactic Plane and Bulge (VPHAS+). Support is provided by the Ministry for the Economy, Development and Tourism, Programa Iniciativa Científica Milenio grant IC120009, awarded to the Millennium Institute of Astrophysics (MAS). We also thank the referee for its comments which greatly improved the present manuscript. A.B. thanks for support from the Millennium Science Initiative (Chilean Ministry of Economy). D.M. is supported by the BASAL Center for Astrophysics and Associated Technologies (CATA) through grant PFB-06, by the Ministry for the Economy, Development and Tourism, Programa Iniciativa Científica Milenio grant IC120009, awarded to the Millennium Institute of Astrophysics (MAS), and by FONDECYT Regular grant No. 1170121.

Software: Matplotlib (Hunter 2007), NumPy (Oliphant 2006), AstroPy (The Astropy Collaboration et al. 2018), Sklearn (Pedregosa et al. 2011), AstroML (Vanderplas et al. 2012), Dophot (Schechter et al. 1993; Alonso-García et al. 2012), VOSA (Bayo et al. 2008), STILTS (Taylor 2006), Spextool Cushing et al. (2004), xtellcorr (Vacca et al. 2003).

Table 5. Information of content of V⁴ Catalog

Column	Units	Description
ID	-	Identification given by the catalog.
Ra ₂₀₀₀	Degrees	Right Ascension of VVV source.
Dec ₂₀₀₀	Degrees	Declination of VVV source.
GLon	Degrees	Galactic longitude of VVV source.
GLat	Degrees	Galactic latitude of VVV source.
\bar{K}_s	mag	Photometric mean value of K _s -band.
\bar{K}_s^{err}	mag	Estimation of \bar{K}_s error using bootstrap technique.
Epochs	-	Observation number of the source in their K _s time serie.
ΔK_s	mag	Photometric total amplitude of K _s -band.
J	mag	Photometric J-band.
J _{err}	mag	Photometric J-band error.
H	mag	Photometric H-band.
H _{err}	mag	Photometric H-band error.
<i>u</i>	mag	Photometric <i>u</i> -band.
<i>u</i> _{err}	mag	Photometric <i>u</i> -band error.
<i>g</i>	mag	Photometric <i>g</i> -band.
<i>g</i> _{err}	mag	Photometric <i>g</i> -band error.
<i>r</i>	mag	Photometric <i>r</i> -band.
<i>r</i> _{err}	mag	Photometric <i>r</i> -band error.
<i>r</i> ²	mag	Photometric <i>r</i> ² -band.
<i>r</i> ² _{err}	mag	Photometric <i>r</i> ² -band error.
<i>i</i>	mag	Photometric <i>i</i> -band.
<i>i</i> _{err}	mag	Photometric <i>i</i> -band error.
H _α	mag	Photometric H _α -band.
H _α err.	mag	Photometric H _α -band error.
η	-	Value of the variability index η .
Class	-	Classification via VVV templates light curve or shape of the time serie.
Tile ID	-	VVV tile where the source is located.
Period	days	Identified period for a VVV source.
A _{K_s}	mag	Extinction measured using Nishiyama et al. (2009) .
Distance	Kpc	Distance measured from PL relations of RRab sources.
CCD	-	Position in (H – K _s , J – H) color-color diagram.
Reference	-	Reference to catalog of a documented source.

APPENDIX

A. BASIC INFORMATION OF V⁴ CATALOG.

Table 6. Parameters of the VVV variables in the V⁴ catalog, description of each column can be found in 5. The complete catalog will be available online.

ID	RAxion	Decxion	Cl _{max}	Cl _{min}	Cl _{int}	K _s	K _s ^{err}	N _{stars}	AK	J	J _{err}	H	H _{err}	u	u _{err}	g	g _{err}	r	r _{err}	r ₂	r _{2,err}	r	r _{err}	i	i _{err}	H _α	H _α ^{err}	τ	Class	ThickD	Period	A _c	Dist	CCD	Reference		
000-1	174.13270153	-63.5879268	204.716587832	-1.01720472064	14.212	0.043	0.0	0.951	-	-	-	-	-	-	-	-	-	-	-	-	-	-	-	-	-	-	-	-	-	-	-	-	-	-	-	-	
000-2	174.14585121	-63.70149127	204.754705209	-2.0240224282	14.84	0.033	0.42	0.852	-	-	-	-	-	-	-	-	-	-	-	-	-	-	-	-	-	-	-	-	-	-	-	-	-	-	-	-	
000-3	174.28300391	-63.36018122	204.781710325	-1.0856805045	14.886	0.03	33	1.295	-	-	-	-	-	-	-	-	-	-	-	-	-	-	-	-	-	-	-	-	-	-	-	-	-	-	-	-	
000-4	174.5486745	-63.51237462	204.787537864	-1.8175121427	13.106	0.06	33	1.295	-	-	-	-	-	-	-	-	-	-	-	-	-	-	-	-	-	-	-	-	-	-	-	-	-	-	-	-	
000-5	174.57906641	-63.40070718	204.790122051	-1.70624030618	15.247	0.058	41	1.439	17.631	0.049	16.346	0.055	-	-	-	-	-	-	-	-	-	-	-	-	-	-	-	-	-	-	-	-	-	-	-	-	
000-6	174.5869225	-63.30788225	204.745873368	-1.61693543228	15.796	0.044	43	1.049	-	-	-	-	-	-	-	-	-	-	-	-	-	-	-	-	-	-	-	-	-	-	-	-	-	-	-	-	
000-7	174.143860	-63.49125342	204.811436522	-1.78472312725	16.224	0.057	41	1.279	17.947	0.05	16.868	0.055	-	-	-	-	-	-	-	-	-	-	-	-	-	-	-	-	-	-	-	-	-	-	-	-	
000-8	174.44546093	-63.78777894	204.960322304	-2.06961609144	14.517	0.04	38	1.033	17.677	0.05	15.829	0.055	-	-	-	-	-	-	-	-	-	-	-	-	-	-	-	-	-	-	-	-	-	-	-	-	
000-9	174.47646923	-63.0580131	204.715017585	-1.36712007129	15.372	0.043	43	1.052	-	-	-	-	-	-	-	-	-	-	-	-	-	-	-	-	-	-	-	-	-	-	-	-	-	-	-	-	
000-10	174.098436	-63.21059924	204.760918008	-1.50906184222	13.841	0.018	43	0.476	14.774	0.048	14.06	0.055	10.021	1.00539	19.124	0.01807	17.793	0.00873	17.719	0.00682	17.037	0.006334	17.1584	0.011451	6.544	ClCeph	0001	129.955	-	-	-	-	-	-	-		
000-11	174.0901457	-63.30755363	204.819055274	-1.68845842086	16.332	0.05	42	1.416	18.11	0.05	17.018	0.059	-	-	-	-	-	-	-	-	-	-	-	-	-	-	-	-	-	-	-	-	-	-	-	-	
000-12	174.0226753	-63.3327279	204.80367017	-1.62681338008	16.037	0.085	41	1.773	-	-	-	-	-	-	-	-	-	-	-	-	-	-	-	-	-	-	-	-	-	-	-	-	-	-	-	-	
000-13	174.51180389	-63.40093742	204.82013197	-1.6909596834	14.93	0.075	37	1.575	17.047	0.049	16.48	0.056	-	-	-	-	-	-	-	-	-	-	-	-	-	-	-	-	-	-	-	-	-	-	-	-	
000-14	174.5188745	-63.51281764	204.81328111	-1.8315067196	15.188	0.018	43	0.504	17.147	0.049	16.004	0.055	-	-	-	-	-	-	-	-	-	-	-	-	-	-	-	-	-	-	-	-	-	-	-	-	
000-15	174.5285331	-63.18521381	204.72720717	-1.48009026299	14.69	0.04	43	1.754	14.879	0.049	14.306	0.055	-	-	-	-	-	-	-	-	-	-	-	-	-	-	-	-	-	-	-	-	-	-	-	-	
000-16	174.5346357	-63.20233576	204.788308391	-1.4919878729	14.654	0.017	39	0.404	-	-	-	-	-	-	-	-	-	-	-	-	-	-	-	-	-	-	-	-	-	-	-	-	-	-	-	-	
000-17	174.5350229	-63.5053082	204.87239933	-1.7831547514	14.654	0.033	43	0.295	15.938	0.049	15.144	0.055	-	-	-	-	-	-	-	-	-	-	-	-	-	-	-	-	-	-	-	-	-	-	-	-	
000-18	174.59579417	-63.67813221	204.903525621	-1.945765066	15.633	0.042	43	1.021	16.838	0.049	15.703	0.055	-	-	-	-	-	-	-	-	-	-	-	-	-	-	-	-	-	-	-	-	-	-	-	-	
000-19	174.5962925	-63.41154026	204.86237627	-1.6925567231	13.445	0.033	44	0.747	15.3	0.049	14.406	0.055	21.1605	1.08495	18.6954	0.011662	17.2673	0.005715	18.0002	0.01598	17.3119	0.00965	17.6514	0.027395	5.56	STV	0001	-	-	-	-	-	-	-	-		
000-20	174.60442126	-63.45118855	204.87687262	-1.72676178017	14.609	0.08	43	0.938	15.921	0.049	15.079	0.055	20.8168	0.008883	20.278	0.045344	19.2298	0.028469	19.2534	0.008609	18.4905	0.024037	18.247	0.045281	0.345	Unclash	0001	-	-	-	-	-	-	-	-	-	
000-25	174.171781737	-63.48811575	204.98455536	-1.7469855882	13.675	0.021	42	0.674	15.217	0.05	14.753	0.04	20.3882	0.080564	19.6707	0.026482	18.4603	0.014426	18.3193	0.017238	17.7066	0.013369	17.6337	0.027176	0.724	STV	0001	-	-	-	-	-	-	-	-	-	
000-26	174.2091611	-63.6881021	205.021024617	-1.9482910251	15.77	0.039	40	1.027	19.081	0.05	17.209	0.058	-	-	-	-	-	-	-	-	-	-	-	-	-	-	-	-	-	-	-	-	-	-	-	-	
000-27	174.7286131	-63.8269181	204.948000319	-1.73983841729	13.83	0.03	42	0.752	-	-	-	-	-	-	-	-	-	-	-	-	-	-	-	-	-	-	-	-	-	-	-	-	-	-	-	-	
000-28	174.5128875	-63.46014602	204.942875661	-1.7178727869	14.867	0.021	43	0.636	17.429	0.03	16.03	0.016	-	-	-	-	-	-	-	-	-	-	-	-	-	-	-	-	-	-	-	-	-	-	-	-	
000-29	174.7452097	-63.3880177	204.90954064	-1.6529316368	14.16	0.025	41	0.641	14.925	0.04	15.90	0.03	-	-	-	-	-	-	-	-	-	-	-	-	-	-	-	-	-	-	-	-	-	-	-	-	
000-30	174.7575568	-63.49116246	204.96712439	-1.74616262187	13.568	0.028	40	0.879	16.3	0.02	14.857	0.06	-	-	-	-	-	-	-	-	-	-	-	-	-	-	-	-	-	-	-	-	-	-	-	-	
000-31	174.789495	-63.72963	205.043483471	-1.97196012303	13.889	0.033	43	0.833	15.666	0.049	14.689	0.05	-	-	-	-	-	-	-	-	-	-	-	-	-	-	-	-	-	-	-	-	-	-	-	-	
000-32	174.79571361	-63.47490768	204.96837603	-1.7288279486	12.934	0.038	42	0.866	15.404	0.049	14.112	0.055	-	-	-	-	-	-	-	-	-	-	-	-	-	-	-	-	-	-	-	-	-	-	-	-	-
000-33	174.81002286	-63.44894789	204.967581872	-1.69011506778	14.127	0.029	43	0.811	16.799	0.049	15.169	0.055	-	-	-	-	-	-	-	-	-	-	-	-	-	-	-	-	-	-	-	-	-	-	-	-	-
000-34	174.81708237	-63.44317121	204.960008881	-1.69280610385	13.876	0.032	42	0.824	15.43	0.049	14.642	0.055	-	-	-	-	-	-	-	-	-	-	-	-	-	-	-	-	-	-	-	-	-	-	-	-	-
000-35	174.830609	-63.4086319	204.98757089	-1.7188806335	15.132	0.044	32	0.903	-	-	-	-	-	-	-	-	-	-	-	-	-	-	-	-	-	-	-	-	-	-	-	-	-	-	-	-	
000-36	174.850516	-63.469396	204.98826538	-1.7145747185	15.348	0.048	31	0.849	-	-	-	-	-	-	-	-	-	-	-	-	-	-	-	-	-	-	-	-	-	-	-	-	-	-	-	-	-
000-37	174.85157043	-63.7092108	205.081204703	-2.0234527097	16.226	0.044	41	1.112	-	-	-	-	-	-	-	-	-	-	-	-	-	-	-	-	-	-	-	-	-	-	-	-	-	-	-	-	
000-38	174.8623778	-63.6894123	204.90557011	-1.7189160608	14.421	0.018	43	0.63	16.126	0.049	15.11	0.055	-	-	-	-	-	-	-	-	-	-	-	-	-	-	-	-	-	-	-	-	-	-	-	-	-
000-39	174.87841157	-62.8692924	204.80730884	-1.1301874516	14.177	0.024	41	0.668	15.157	0.049	14.619	0.055	20.5883	0.096708	18.543	0.011593	17.3772	0.0061109	17.6678	0.00628	17.1084	0.006615	17.3543	0.012201	2.564	Rbab	0001	0.395346	0.388	5.892	-	-	-	-	-		
000-40	174.887108	-62.988212	204.871109473	-1.2460192286	13.363	0.031	40	0.667	14.748	0.048	14.118	0.055	-	-	-	-	-	-	-	-	-	-	-	-	-	-	-	-	-	-	-	-	-	-	-	-	
000-41	174.0054348	-63.7297262	205.089173901	-1.9701617451	15.01	0.018	44	0.395	16.275	0.049	15.453	0.055	-	-	-	-	-	-	-	-	-	-	-	-	-	-	-	-	-	-	-	-	-	-	-	-	
000-42	174.91757563	-63.0508362	204.90472739	-1.3030081895	15.2	0.059	44	1.441	17.221	0.052	16.048	0.057	-	-	-	-	-	-	-	-	-	-	-	-	-	-	-	-	-	-	-	-	-	-	-	-	
000-43	174.9375784	-63.46692966	205.027169272	-1.70078633295	14.149	0.043	43	0.936	15.276	0.049	14.322	0.055	-	-	-	-	-	-	-	-	-	-	-	-	-	-	-	-	-	-	-	-	-	-	-	-	
000-44	175.04919391	-63.4702168	205.06834462	-1.70144196223	15.48	0.085	43	1.616	15.912	0.049	15.106	0.055	-	-	-	-	-	-	-	-	-	-	-	-	-	-	-	-	-	-	-	-	-	-	-	-	-
000-45	175.21207019	-63.1614867	205.132071225	-1.6188242178	15.826	0.074	34	1.361	-	-	-	-	-	-	-	-	-	-	-	-	-	-	-	-	-	-	-	-	-	-	-	-	-	-	-	-	
000-46	175.28487967	-62.95803377	205.039895249	-1.6846143672																																	

REFERENCES

- Alonso-García, J., Dékány, I., Catelan, M., et al. 2015, *AJ*, 149, 99
- Alonso-García, J., Mateo, M., Sen, B., et al. 2012, *AJ*, 143, 70
- Angeloni, R., Contreras Ramos, R., Catelan, M., et al. 2014, *A&A*, 567, A100
- Arnaboldi, M., Neeser, M. J., Parker, L. C., et al. 2007, *The Messenger*, 127
- Arnaboldi, M., Rejkuba, M., Retzlaff, J., et al. 2012, *The Messenger*, 149, 7
- Bailey, S. I. 1902, *Annals of Harvard College Observatory*, 38
- Barbá, R. H., Roman-Lopes, A., Nilo Castellón, J. L., et al. 2015, *A&A*, 581, A120
- Bayo, A., Rodrigo, C., Barrado Y Navascués, D., et al. 2008, *A&A*, 492, 277
- Bessell, M. S., & Brett, J. M. 1988, *PASP*, 100, 1134
- Bonatto, C., & Bica, E. 2010, *A&A*, 516, A81
- Borissova, J., Bonatto, C., Kurtev, R., et al. 2011, *A&A*, 532, A131
- Borissova, J., Chené, A.-N., Ramírez Alegría, S., et al. 2014, *A&A*, 569, A24
- Borissova, J., Ramírez Alegría, S., Alonso, J., et al. 2016, *AJ*, 152, 74
- Bressan, A., Marigo, P., Girardi, L., et al. 2012, *MNRAS*, 427, 127
- Carpenter, J. M., Hillenbrand, L. A., & Skrutskie, M. F. 2001, *AJ*, 121, 3160
- Chené, A.-N., Borissova, J., Clarke, J. R. A., et al. 2012, *A&A*, 545, A54
- Chené, A.-N., Borissova, J., Bonatto, C., et al. 2013, *A&A*, 549, A98
- Cody, A. M., Stauffer, J., Baglin, A., et al. 2014, *AJ*, 147, 82
- Contreras Peña, C., Lucas, P. W., Minniti, D., et al. 2017a, *MNRAS*, 465, 3011
- Contreras Peña, C., Lucas, P. W., Kurtev, R., et al. 2017b, *MNRAS*, 465, 3039
- Cross, N. J. G., Collins, R. S., Mann, R. G., et al. 2012, *A&A*, 548, A119
- Cushing, M. C., Vacca, W. D., & Rayner, J. T. 2004, *PASP*, 116, 362
- Dalton, G. B., Caldwell, M., Ward, A. K., et al. 2006, in *Proc. SPIE*, Vol. 6269, Society of Photo-Optical Instrumentation Engineers (SPIE) Conference Series, 62690X
- Dékány, I., Minniti, D., Majaess, D., et al. 2015, *ApJL*, 812, L29
- Dong, H., Schödel, R., Williams, B. F., et al. 2017, *MNRAS*, 471, 3617
- Drake, A. J., Djorgovski, S. G., Mahabal, A., et al. 2009, *ApJ*, 696, 870
- Drew, J. E., Gonzalez-Solares, E., Greimel, R., et al. 2014, *MNRAS*, 440, 2036
- Elorrieta, F., Eyheramendy, S., Jordán, A., et al. 2016, *A&A*, 595, A82
- Elson, R. A. W., Fall, S. M., & Freeman, K. C. 1987, *ApJ*, 323, 54
- Findeisen, K., Hillenbrand, L., Ofek, E., et al. 2013, *ApJ*, 768, 93
- Gavrilchenko, T., Klein, C. R., Bloom, J. S., & Richards, J. W. 2014, *MNRAS*, 441, 715
- Graczyk, D., & Eyer, L. 2010, *AcA*, 60, 109
- Gran, F., Minniti, D., Saito, R. K., et al. 2016, *A&A*, 591, A145
- Harju, J., Lehtinen, K., Booth, R. S., & Zinchenko, I. 1998, *A&AS*, 132, 211
- Herbig, G. H. 1966, *Vistas in Astronomy*, 8, 109
- Herbig, G. H. 1989, in *European Southern Observatory Conference and Workshop Proceedings*, Vol. 33, European Southern Observatory Conference and Workshop Proceedings, ed. B. Reipurth, 233–246
- Hervé, A., Martins, F., Chené, A.-N., Bouret, J.-C., & Borissova, J. 2016, *NewA*, 45, 84
- Higuchi, A. E., Sato, A., Tsukagoshi, T., et al. 2017, *ApJL*, 839, L14
- Hillenbrand, L. A., Strom, S. E., Vrba, F. J., & Keene, J. 1992, *ApJ*, 397, 613
- Huijse, P., Estevez, P. A., Zegers, P., Principe, J. C., & Protopapas, P. 2011, *IEEE Signal Processing Letters*, 18, 371
- Hunter, J. D. 2007, *Computing In Science & Engineering*, 9, 90
- Kaiser, N., Aussel, H., Burke, B. E., et al. 2002, in *Proc. SPIE*, Vol. 4836, Survey and Other Telescope Technologies and Discoveries, ed. J. A. Tyson & S. Wolff, 154–164
- Kalari, V. M., Vink, J. S., Drew, J. E., et al. 2015, *MNRAS*, 453, 1026
- Krabbendam, V. L., & Sweeney, D. 2010, in *Proc. SPIE*, Vol. 7733, Ground-based and Airborne Telescopes III, 77330D
- Kwok, S., Volk, K., & Bidelman, W. P. 1997, *ApJS*, 112, 557
- Lomb, N. R. 1976, *Ap&SS*, 39, 447
- Lumsden, S. L., Hoare, M. G., Urquhart, J. S., et al. 2013, *ApJS*, 208, 11

- Marigo, P., Girardi, L., Bressan, A., et al. 2017, *ApJ*, 835, 77
- McSwain, M. V., & Gies, D. R. 2005, *ApJS*, 161, 118
- Meyer, M. R., Calvet, N., & Hillenbrand, L. A. 1997, *AJ*, 114, 288
- Minniti, D., Lucas, P. W., Emerson, J. P., et al. 2010, *NewA*, 15, 433
- Minniti, D., Contreras Ramos, R., Alonso-García, J., et al. 2015, *ApJL*, 810, L20
- Minniti, D., Dékány, I., Majaess, D., et al. 2017, *AJ*, 153, 179
- Mottram, J. C., Hoare, M. G., Urquhart, J. S., et al. 2011, *A&A*, 525, A149
- Navarete, F., Daminieli, A., Barbosa, C. L., & Blum, R. D. 2015, *MNRAS*, 450, 4364
- Navarro Molina, C., Borissova, J., Catelan, M., et al. 2016, *MNRAS*, 462, 1180
- Nishiyama, S., Tamura, M., Hatano, H., et al. 2009, *ApJ*, 696, 1407
- Ojha, D. K., Tamura, M., Nakajima, Y., et al. 2004, *ApJ*, 616, 1042
- Oliphant, T. 2006, *Guide to NumPy*
- Palma, T., Minniti, D., Dékány, I., et al. 2016, *NewA*, 49, 50
- Pedregosa, F., Varoquaux, G., Gramfort, A., et al. 2011, *Journal of Machine Learning Research*, 12, 2825
- Perryman, M. A. C. 2005, in *Astronomical Society of the Pacific Conference Series*, Vol. 338, *Astrometry in the Age of the Next Generation of Large Telescopes*, ed. P. K. Seidelmann & A. K. B. Monet, 3
- Pojmanski, G. 1998, *AcA*, 48, 35
- Rebull, L. M., Cody, A. M., Covey, K. R., et al. 2014, *AJ*, 148, 92
- Saito, R. K., Minniti, D., Dias, B., et al. 2012a, *A&A*, 544, A147
- Saito, R. K., Hempel, M., Minniti, D., et al. 2012b, *A&A*, 537, A107
- Sana, H., James, G., & Gosset, E. 2011, *MNRAS*, 416, 817
- Scargle, J. D. 1982, *ApJ*, 263, 835
- Schechter, P. L., Mateo, M., & Saha, A. 1993, *PASP*, 105, 1342
- Schmidt-Kaler, T. 1982, *Bulletin d'Information du Centre de Données Stellaires*, 23, 2
- Shin, M.-S., Sekora, M., & Byun, Y.-I. 2009, *MNRAS*, 400, 1897
- Skrutskie, M. F., Cutri, R. M., Stiening, R., et al. 2006, *AJ*, 131, 1163
- Smith, L. C., Lucas, P. W., Kurtev, R., et al. 2018, *MNRAS*, 474, 1826
- Sokolovsky, K. V., Gavras, P., Karamelas, A., et al. 2017, *MNRAS*, 464, 274
- Stetson, P. B. 1996, *PASP*, 108, 851
- Taylor, M. B. 2006, in *Astronomical Society of the Pacific Conference Series*, Vol. 351, *Astronomical Data Analysis Software and Systems XV*, ed. C. Gabriel, C. Arviset, D. Ponz, & S. Enrique, 666
- The Astropy Collaboration, Price-Whelan, A. M., Sipőcz, B. M., et al. 2018, *ArXiv e-prints*, arXiv:1801.02634
- Thompson, R. 1985, *Journal of the Royal Statistical Society. Series B (Methodological)*, 47, 53.
<http://www.jstor.org/stable/2345543>
- Vacca, W. D., Cushing, M. C., & Rayner, J. T. 2003, *PASP*, 115, 389
- Vanderplas, J., Connolly, A., Ivezić, Ž., & Gray, A. 2012, in *Conference on Intelligent Data Understanding (CIDU)*, 47–54
- von Neumann, J. 1941, *Ann. Math. Statist.*, 12, 367.
<http://dx.doi.org/10.1214/aoms/1177731677>
- Welch, D. L., & Stetson, P. B. 1993, *AJ*, 105, 1813
- Wolk, S. J., Rice, T. S., & Aspin, C. 2013, *ApJ*, 773, 145
- Zechmeister, M., & Kürster, M. 2009, *A&A*, 496, 577